Reverting chemoresistance of targeted agents by a ultrasoluble dendritic nanocapsule

Qida Hu, Wangteng Wu, Meng Wang, Shiyi Shao, Piaopiao Jin, Qi Chen, Hongzhen Bai, Xinyu Zhao, Junming Huang, Jianwei Wang, Guping Tang, Tingbo Liang

PII: S0168-3659(19)30670-4

DOI: https://doi.org/10.1016/j.jconrel.2019.11.020

Reference: COREL 10025

To appear in: *Journal of Controlled Release*

Received date: 2 August 2019

Revised date: 2 November 2019

Accepted date: 17 November 2019

Please cite this article as: Q. Hu, W. Wu, M. Wang, et al., Reverting chemoresistance of targeted agents by a ultrasoluble dendritic nanocapsule, *Journal of Controlled Release* (2018), https://doi.org/10.1016/j.jconrel.2019.11.020

Reverting Chemoresistance of Targeted Agents by a Ultrasoluble Dendritic Nanocapsule

Qida Hu[a,1], Wangteng Wu[a,b,1], Meng Wang[a], Shiyi Shao[a], Piaopiao Jin[c], Qi Chen[b], Hongzhen Bai[b], Xinyu Zhao[a], Junming Huang[a], Jianwei Wang[b], Guping Tang[b,*], and Tingbo Liang[a,d,e,**]

[a] Department of Hepatobiliary and Pancreatic Surgery, First Affiliated Hospital, Zhejiang University School of Medicine, Hangzhou 310003, China

[b] Institute of Chemical Biology and Pharmaceutical Chemistry, Zhejiang University, Hangzhou 310028, China

[c] Health Promotion Centre, First Affiliated Hospital, Zhejiang University School of Medicine, Hangzhou 310003, China

[d] Innovation Center for the Study of Pancreatic Diseases, Zhejiang Province

[e] Zhejiang Provincial Key Laboratory of Pancreatic Disease

*Corresponding author.

**Corresponding author.

E-mail addresses: tangguping@zju.edu.cn (G. Tang), liangtingbo@zju.edu.cn (T. Liang).

[1] These authors contributed equally to this work.

ABSTRACT

Malignancies treated by insoluble targeted agents show low dose exposure and therapeutic responses, therefore easily develop drug resistance. Nanoparticle-modified drugs might disrupt chemoresistance by increasing dose exposure and altering resistance pathways, as administrated *via* the intravenous route to maximize efficacy. Herein, we proposed a self-assembled nanocapsulation strategy to construct a nanocomplex with multiarm polymer and novel dendrimer series (MAP-mG3) for encapsulating insoluble inhibitors by nucleotide lock. MAP-mG3 delivering the mammalian target of rapamycin (mTOR) inhibitor OSI-027 (MAP-mG3/OSI-027) showed higher loading capacity, enhanced solubility, controlled release, and increased intracellular tumoral accumulation. MAP-mG3/OSI-027, more efficiently than the free targeted agents, attenuated mTOR phosphorylation and inhibited growth of pancreatic cancer cells. In addition, MAP-mG3/OSI-027 reverted chemoresistance to OSI-027 in drug resistance pancreatic cancer by increasing intracellular dose exposure, as well as regulating ABCB1 expression and compensatory pathways. The optimized nanocapsulation design provides an effective strategy to engineer and reactivate insoluble targeted agents for chemoresistant applications.

KEYWORDS: targeted agents, dendritic nanocapsule, functional delivery, chemoresistance

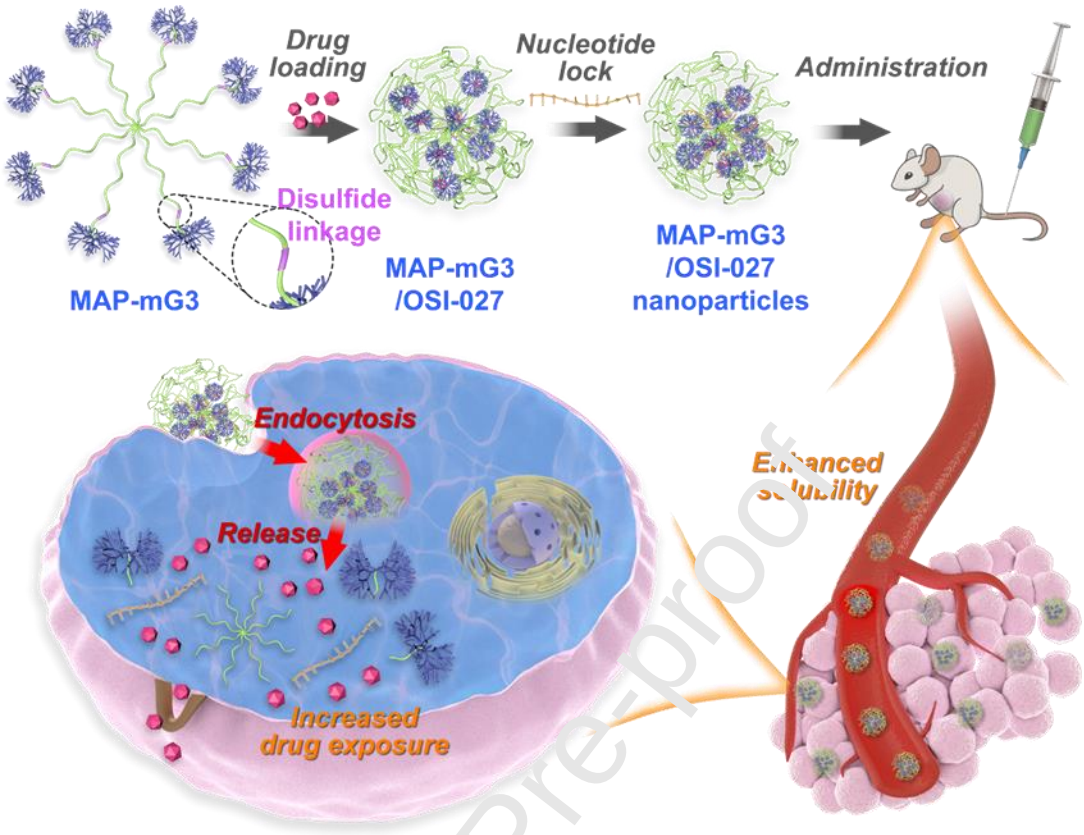

Scheme 1. Schematic illustration of MAP-mG3/OSI-027 system for pancreatic cancer: intravenous injection, tumoral accumulation, redox-response and overcome drug resistance.

1. Introduction

Various targeted agents have been developed to inhibit specifically the molecular pathways driving tumor proliferation[1]. We previously found that inhibition of mammalian target of rapamycin (mTOR) expression can suppress proliferation of pancreatic cancer cells *in vitro* and reverse the immunosuppressive microenvironment to facilitate an immunologic effect *in vivo*[2]. Nevertheless, many patients with mTOR mutations have an unsatisfactory response (or even disease progression) after treatment using orally-administrated insoluble targeted agents[3, 4]. The limited response to treatment might be associated with a relatively low exposure dose, which is mainly caused by poor solubility in the tumor microenvironment. Also, long-term constrained efficacy would generate drug resistance in surviving cancer cells, with altered activation of compensatory pathways[5, 6].

An approach to increase the locoregional exposure dose and to overcome drug resistance is required urgently. Several previous applications have raised the feasibility[7, 8]. For instance, nab-paclitaxel, a albumin-conjugated paclitaxel therapeutic, improved solubility and pharmacodynamics, thus making it the first-line treatment for pancreatic cancer[8]. More importantly, nanoparticle-modified drugs, which could be administrated *via* intravenous route to maximize efficacy, might disrupt chemoresistance by increasing dose exposure and altering resistance pathways[5, 9].

We have previously designed a dendrimer-based nanoparticle modified with polyethylene glycol (PEG) *via* a redox response linkage termed "multiarm polymer complex with dendrimer" (MAP-dendrimer)[10]. Specifically, the nanoparticle packs the hydrophobic chemotherapeutic agent (doxorubicin) and model nucleotides in a condensed form simultaneously. This strategy enables protection of the loaded dendrimer cores during systemic delivery, and release of the cargo upon lysosomal stimulation. Therefore, an updated strategy might enable the required functional delivery of insoluble targeted agents, by forming drug-embedded nanocapsules, but with more loading space to achieve greater viable dose in the tumor microenvironment.

Herein, we proposed a self-assembled nanocapsulation strategy to construct a nanocomplex with multiarm PEG and a novel dendrimer for encapsulating insoluble mTOR inhibitors by nucleotide lock. The previously adapted lowest-generation dendrimers (modified second

generation, denoted as "mG2") were least cytotoxic, but with limited loading capacity[11-13]. High loading capacity and tolerable cytotoxicity are concurrently required[14]. In the present study, we synthesized a new third-generation dendrimer, modified G3 dendrimer (mG3) and the MAP-mG3 nanocapsule system, to investigate the feasibility of functional delivery and therapeutic effect for targeted agents to revert chemoresistance.

2. Results

2.1 Chemical optimization of the multiarm polymer complex with dendrimer (MAP-dendrimer)

The new MAP-mG3 nanocapsule was synthesized by conjugating overdosed mG3 dendrimers to the ends of an eight-arm PEG scaffold (Fig. 1a and Fig. S1), followed by encapsulation of targeted agents and nucleotide condensation driven by electrostatic interference. To ensure favorable pharmacokinetics, each arm of the PEG scaffold contained a disulfide linkage synthesized by modification of the eight-arm PEG chain end with an N-hydroxysuccinimide (NHS)-terminal PEG bridged by cystamine dihydrochloride, to engineer the redox-responsiveness potential. Encapsulation of the targeted agents decreased the hydrophilicity of the loaded dendrimers, but not the PEG scaffold, causing an inequality in hydrophilicity in the dendrimers and PEG[10]. The hydrophobic dendrimers loaded with targeted agents moved gradually to the inside layer, whereas the hydrophilic PEG scaffold became the outside layer spontaneously to form the MAP-mG3 nanocapsules (Fig. 1b). This synthetic approach could be applied for encapsulation of most hydrophobic targeted agents, including mTOR inhibitors. In the current study, we used OSI-027, an insoluble mTOR inhibitor, for efficacy validation of the MAP-mG3 nanocapsule system.

To determine the loading of MAP-dendrimers series for mTOR inhibitors, we investigated the encapsulation rate of OSI-027 by ultraviolet spectrometry of OSI-027-loaded MAP-dendrimers (Fig. 1c). For comparison purpose, we also synthesized a control series of MAP complexes with poly(amidoamine) dendrimers (PAMAM), namely the MAP complex with second- or third-generation PAMAM (MAP-pG2 or MAP-pG3). The MAP complex with G3 dendrimers had a superior loading rate for OSI-027 than the complex with G2 dendrimers (14.2% in MAP-mG3 *vs*. 9.8% in MAP-mG2; 6.2% in MAP-pG3 *vs*. 3.1% in MAP-pG2). The MAP complexes with

modified dendrimers showed a universally higher loading rate compared with the MAP complexes with PAMAM dendrimers. A simulated model of drug–dendrimer interference also suggested that the mG3 dendrimers had a relatively lower inhibition constant (K_i) of 65.48 fM (Fig. 1d and Fig. S2), which was inversely correlated with the strength of the drug–dendrimer interaction, thereby confirming the loading capacity of the MAP-mG3 system.

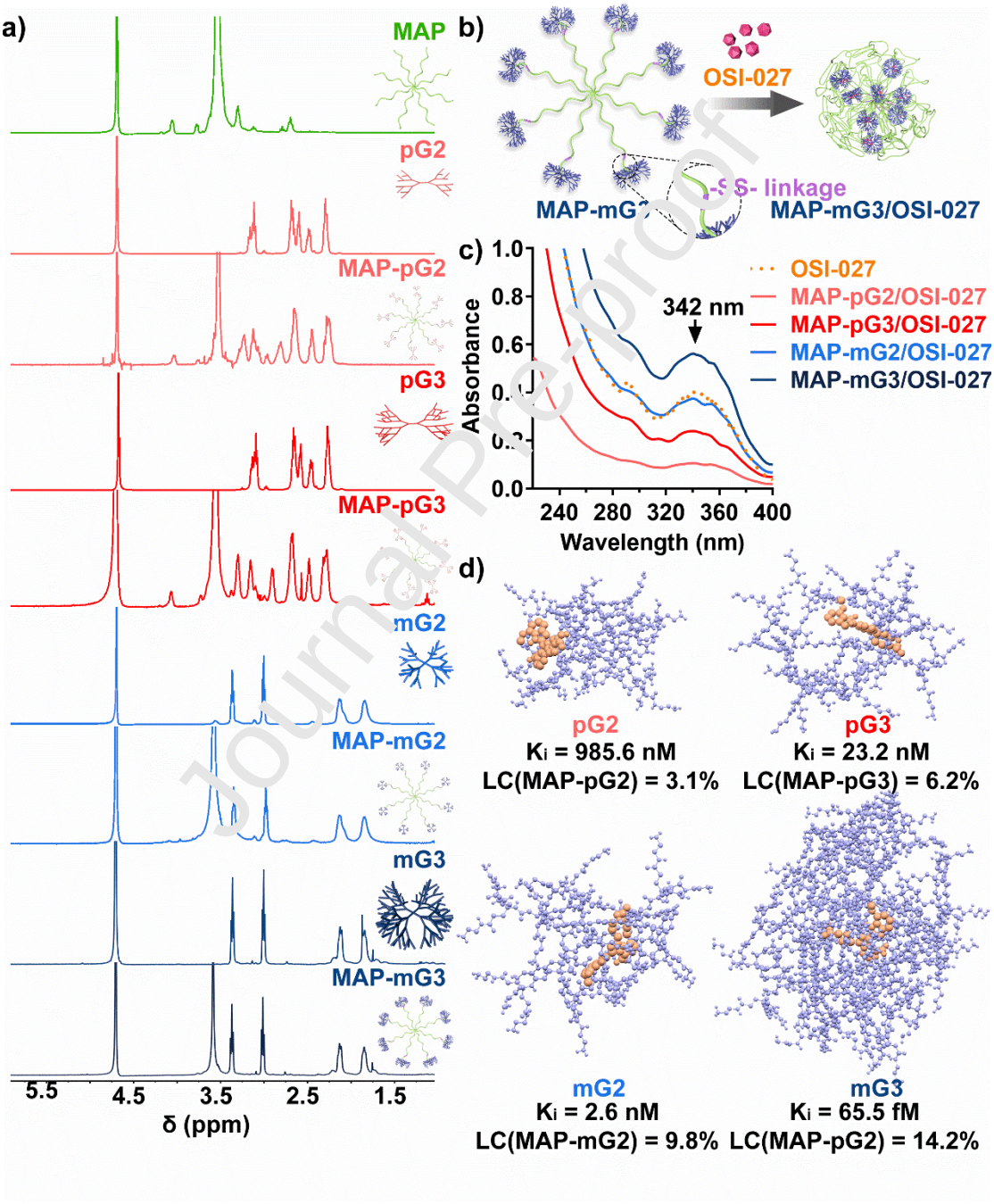

Figure 1. Chemical synthesis and characterization of multiarm polymer complex with dendrimer (MAP-dendrimer). a) ^{1}H NMR spectrum of the dendrimer components [second- and third-generation poly(amidoamine) dendrimers (pG2 and pG3, respectively) and modified second- and third-generation dendrimers (mG2 and mG3, respectively)] and the corresponding series of MAP-dendrimer complexes. b) Synthesis of a representative MAP-dendrimer (MAP-mG3). c) Ultraviolet spectrum of the targeted agent OSI-027 (orange dotted dash), and a series of OSI-027-loaded MAP-dendrimer complexes. The arrow indicates the absorbance peak of OSI-027 at 342 nm. d) Loading capacity of MAP-dendrimers and simulated interaction between dendrimer components (light-purple) and OSI-027 (gold) with demonstration of the inhibition constant (K_i).

2.2. Formation of ultrasoluble MAP-dendrimer/OSI-027 nanocapsules

Transmission electron microscopy (TEM) and dynamic light scattering (DLS) demonstrated spontaneous encapsulation of OSI-027 into nanoparticles with condensation of nucleotides, such as siRNA, at an nitro:phosphonium (N:P) ratio >3 (Fig. 2a). The N:P ratio portrayed the constitution of cationic materials and anionic nucleotides which must be optimized. Spherical structures of MAP-mG3/OSI-027 nanocapsules were observed by TEM to have a particle radius (mean ± s.d.) of 171.1 ± 10.8 nm (n = 30) at an N:P ratio of 10, similar to MAP-mG2/OSI-027 (166.1 ± 7.6 nm) (n = 30) (Fig. 2b). DLS further confirmed the narrow size distribution of MAP-mG3/OSI-027 nanocapsules with a radius of 170.6 ± 22.9 nm (n = 3), which was comparable with that of MAP-mG2/OSI-027 (164.3 ± 19.7 nm) (n = 3) (Fig. S4a). DLS also showed the cationic feature of MAP-mG3/OSI-027 nanocapsules with a ζ-potential of 10.0 ± 0.7 mV (Fig. S4b), which reduced inter-particle aggregation. Both results suggested that dendrimer generation had little impact on the physical attributes of the drug-loaded nanocapsules. The nanocapsules were stable in size and polydispersity in a neutral environment without reduction stimuli, whereas polydispersity in the presence of the reducing agent dithiothreitol (DTT) increased with time (Fig. S5). These observations suggested that the nanocapsules should exist stably in the systemic circulation but disassemble gradually with cleavage of disulfide bonds after reduction.

To confirm the best nanocapsule candidates and delivery condition for further characterization and subsequent applications, we then investigated transfection efficacy based on expression of enhanced green fluorescent protein (EGFP) using MAP-mG3/OSI-027 in comparison with other homologs (MAP-pG2, MAP-pG3, and MAP-mG2) (Fig. 2c). Though all the nanocapsule candidates were capable of EGFP transfection and featured with similar minor cytotoxicity (Fig. S6), MAP-mG3/OSI-027 nanocapsules showed best efficacy at an N:P ratio of 10 with 20.8%

expression in transfected Panc-02 cells (Fig. 2c and Fig. S7a). This result was verified by a significantly higher expression intensity of $5.0 \times 10^8 \pm 1.4 \times 10^8$ RLU/mg protein (n = 3) in the luciferase reporter assay ($p = 0.002$, *vs.* $1.6 \times 10^8 \pm 1.4 \times 10^7$ RLU/mg protein for MAP-mG2, one-way ANOVA followed by Tukey's post hoc test; n = 3) (Fig. 2d and Fig. S7b). Meanwhile, we characterized cellular uptake and intracellular trafficking mediated by the nanocapsule candidates with visualization from fluorescein isothiocyanate (FITC)-labelled fluorescent nc-siRNA using confocal laser scanning microscopy. All nanocapsule candidates showed satisfactory internalization and were retained in cytoplasm rather than the nucleus in 4 h (Fig. 2e). Such internalization might enable sustained release of the cargo agent with prolonged retention of the nanocapsules, as illustrated previously by our research team[10]. Interestingly, MAP-mG3/OSI-027 showed significantly superior mean fluorescence intensity after internalization as measured by flow cytometry compared with other candidates ($p < 0.001$, one-way ANOVA followed by Tukey's test) (Fig. 2f). Within a tolerated dose, MAP-mG3/OSI-027 nanocapsules were the best for transfection and internalization among the homolog candidates. mG3, with denser positive charges than the other homologs, facilitates the membrane penetration and lysosomal escape associated with better transfection and internalization[15], which could promote MAP-mG3 delivery. Therefore, we selected MAP-mG3 with an optimized N:P ratio of 10 for subsequent studies on OSI-027 delivery with evidence of enhanced efficacy at the cellular level.

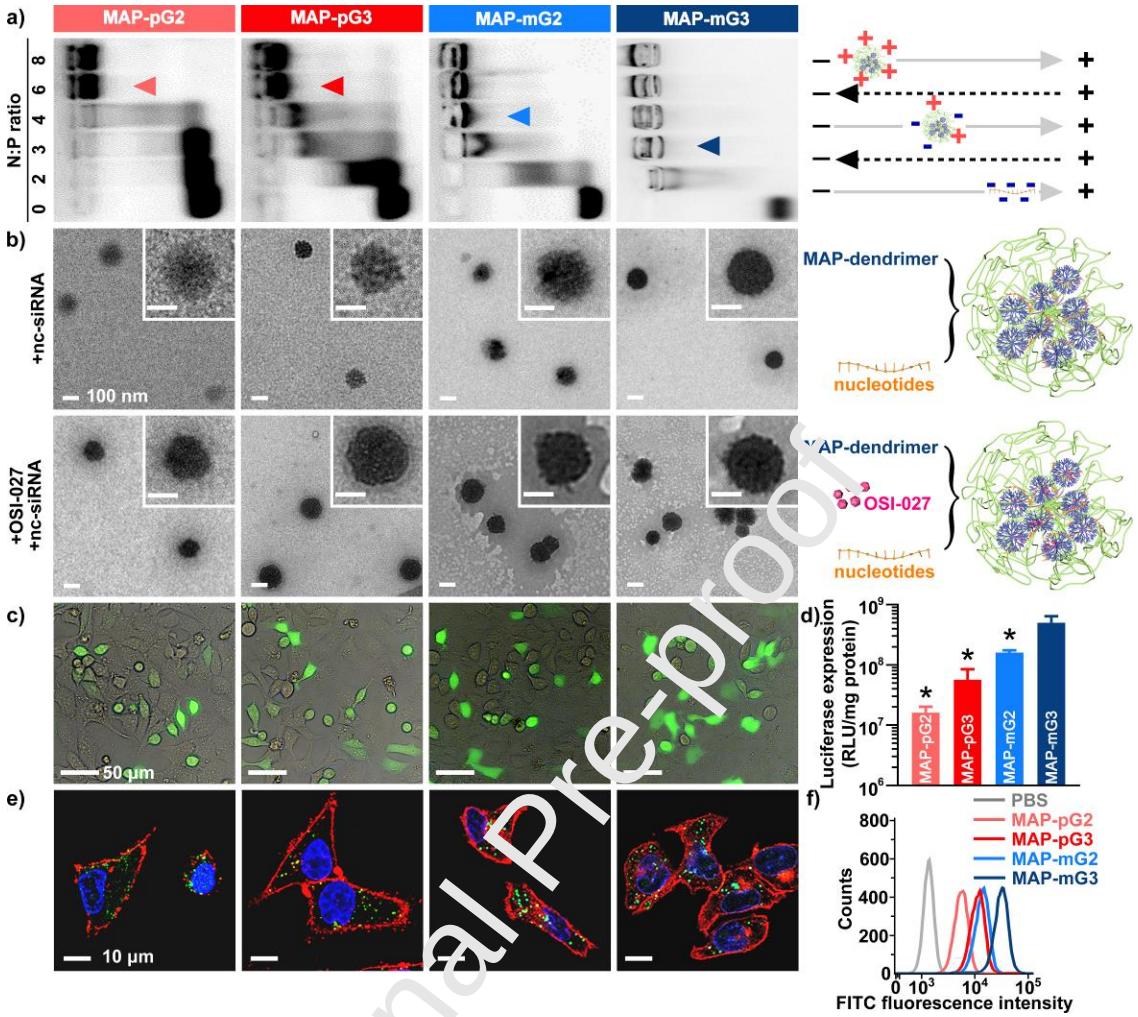

Figure 2. Formation of a MAP-dendrimer system after nucleotide condensation. a) The ability to condense nucleotides with MAP-dendrimer complexes characterized by agarose gel electrophoresis. The triangles indicate the lowest nitro:phosphonium (N:P) ratios required to completely condense negative control siRNA (nc-siRNA) nucleotides. Dashed line (black) and solid line (grey) represent electric filed and electrophoresis directions, respectively. b) Representative transmission electron microscopy (TEM) photographs of MAP-dendrimers with nc-siRNA and MAP-dendrimers with both nc-siRNA and OSI-027. Formation of the MAP-dendrimer system is shown schematically on the right panel. The bar represents 100 nm. c) Representative photographs of Panc-02 cells after enhanced green fluorescence protein plasmid (pEGFP) transfection using MAP-dendrimer/OSI-027 complexes. The bar represents 50 μm. d) Transcriptional activity in Panc-02 cells after transfection by the MAP-dendrimer/OSI-027 series in luciferase reporter assays. RLU, relative luminescence unit. *$p < 0.001$, *vs.* MAP-mG3, one-way ANOVA followed by Tukey's *post hoc* test. e) Cellular uptake of the MAP-dendrimer system carrying nc-siRNA labelled with fluorescein isothiocyanate (FITC; green) in Panc-02 cells visualized by confocal laser scanning microscopy. The cell membrane and nucleus are stained by Alexa Fluor® 647 (red) and DAPI (blue), respectively. The bar represents 10 μm. f)

Pattern of FITC fluorescence intensity by flow cytometry in Panc-02 cells after internalization of the MAP-dendrimer system carrying FITC-labelled nc-siRNA.

2.3. MAP-mG3/OSI-027 nanocapsules mediate functional cargo delivery and increase drug exposure dose

Enhancement of the bioavailability of OSI-027 requires several major functions. An improvement in solubility with nanoparticle encapsulation should be the first requirement for a high dose of insoluble OSI-027 to be distributed in a soluble form in tumor microenvironments. The viable dose of OSI-027 (15.9 ± 1.6 μg/mL) for free OSI-027 (n = 3) increased by 53.8-fold to 870.9 ± 23.2 μg/mL (n = 3) in MAP-mG3/OSI-027 ($p < 0.001$, Student's t-test) (Fig. 3a), which demonstrated our MAP-mG3 design had increased solubility. Increased solubility also facilitated bioviability of OSI-027 with improved pharmacokinetics. The maximal plasma concentration (C_{max}) was 117.8 ± 29.5 μg/mL (n = 3) at 1 hour post injection, and sustained above 30 μg/mL within 12 hours (Fig S8), at least two-fold of the C_{max} value in the previously published preclinical and clinical trial studies [16, 17].

As the second requirement, functional liberation of free drug from the MAP-mG3 nanocapsules addresses the redox-sensitive cleavage of the disulfide bond and subsequent intracellular release from the dendrimers. To verify the response to reducing stimuli, we measured the time-dependent cumulative release of OSI-027 with high-performance liquid chromatography (HPLC). In comparison with minor release of OSI-027 in an environment free of reducing stimuli [maximum cumulative release (R%) = 39.4, 95% CI 37.6–41.4], significantly increased cumulative release was demonstrated upon DTT stimulation (R% = 83.1, 95% CI 80.3–85.9; F = 433.5, $p < 0.001$, *vs.* DTT-free, extra sum-of-squares F test) with a first-order half-life of 1.6 h (95% CI 1.4–1.7) (Fig. 3b). Meanwhile, nanocapsules under a DTT stimulus had an increased particle radius of 457.9 ± 65.6 nm (n = 3) according to DLS (Fig. S5). These data demonstrated controlled release at an appreciable rate and a stimuli-related change in particle size in reduction circumstances that mimicked endolysis. In addition, the pancreatic cancer microenvironment has a higher level of reduced glutathione hormone (GSH)[18], another reduction stimulus that might also cause controlled release of cargo drugs. Previously, we showed that our design using disulfide bonds had high sensitivity to reduction stimuli in preclinical studies[10, 18, 19]. Hence, the redox-responsive release and morphologic change of

our updated design showed responsiveness potential in a pancreatic cancer model. Additionally, the nanocapsules without nc-siRNA nucleotide lock demonstrated robust OSI-027 release with a significantly shorter half-life of 0.47 h (95% CI 0.41–0.53; F = 105.1, $p < 0.001$, *vs.* MAP-mG3/OSI-027 with nc-siRNA lock, extra sum-of-squares F test), addressing the necessity of nucleotide lock inclusion to avoid drug release before arriving at the target site.

With redox-responsiveness verified by a simple model of two-compartment release, our nanocapsule delivery system would eventually require another functional requirement to ensure a viable intracellular dose: enhanced accumulation of the intracellular cargo. HPLC was used to determine the intercellular OSI-027 concentration in lysed Panc-02 cells (Fig. 3c). Incubation with MAP-mG3/OSI-027 doubled the intracellular accumulation of OSI-027 compared with incubation with free OSI-027 within 4 h ($p < 0.001$ for 5 μM or 10 μM of OSI-027 equivalent, MAP-mG3/OSI-027 *vs.* free OSI-027, one-way ANOVA followed by Tukey's post hoc test) in a dose-dependent and time-dependent manner ($p < 0.001$, 5 μM *vs.* 10 μM MAP-mG3/OSI-027, two-way ANOVA followed by Bonferroni's test). Enhancement of total intracellular accumulation would lead to an improved focal dose and therapeutic effect of the cargo agent[20]. Increased intracellular accumulation of the cargo agent might help overcome simultaneous effluence in stressed cells by several mechanisms, such as "pumping out" the excessive drug, which facilitates drug resistance gradually[21].

Intratumoral accumulation and excessive distribution of the cargo agent *in vivo* is also a functional requirement that is equally important as intracellular accumulation. Distribution of a delivery system in Panc-02 tumor-bearing mice (C57BL/6) was assessed by Cy5 fluorescence labelled on the MAP-mG3/OSI-027 nanocapsule observed by an *in vivo* imaging system in a time-dependent way (Fig. 3d). MAP-mG3 mediated high tumoral fluorescence 2 h after tail-vein injection that was retained for the following 8 h (43.7 ± 5.3% of expression after 2 h) (n = 3), indicating excessive and persistent accumulation within the tumor, whereas free Cy5 nc-siRNA achieved 40.3 ± 3.2% (n = 3) 8 h after injection. Further pharmacodynamic investigation with HPLC quantification showed a significantly enhanced distribution of MAP-mG3/OSI-027 in tumors, which was 15.9 fold of the drug accumulation in the tumors treated with oral OSI-027 ($p < 0.001$, Student's t test) at 12 hours post administration (Fig. 3e). The optimized distribution mediated by MAP-mG3 was enabled by the enhanced permeability and retention effect. The

latter helped to increase intratumoral therapeutic accumulation of the cargo agents in systemic treatment and lowered exposure to normal tissue simultaneously, leading to minor side effects[22, 23].

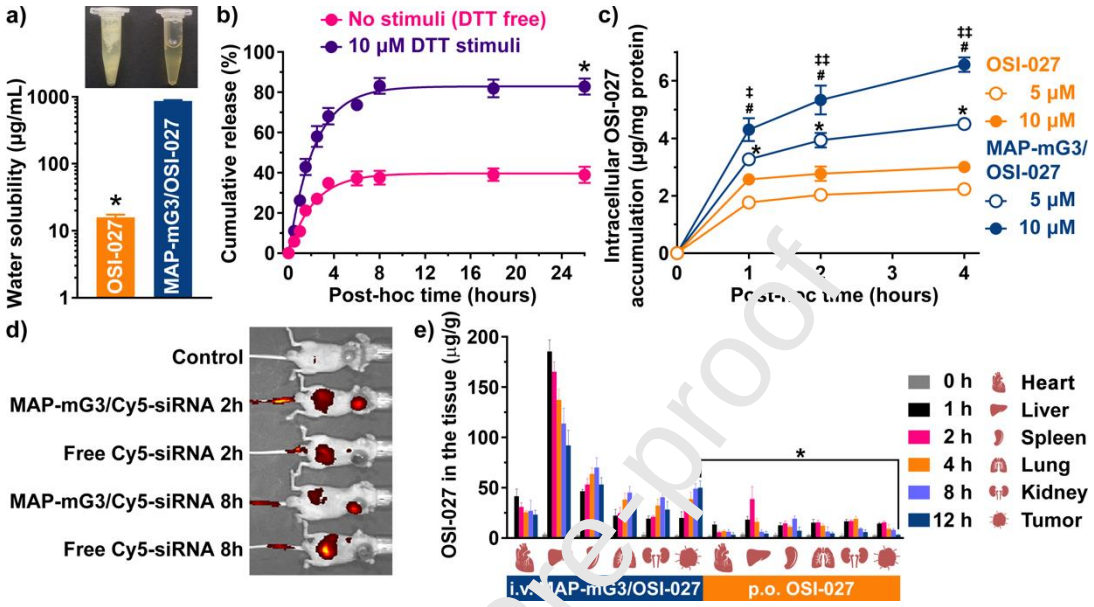

Figure 3. Major functions of the MAP-mG3 system. a) Enhanced water solubility. The photograph demonstrates a mixture of 0.5 mL of water plus 400 μg of OSI-027 (left) and the solution of equivalent MAP-mG3/OSI-027 in 0.5 mL of water (right). *p < 0.001, *vs.* MAP-mG3/OSI-027, Student's *t*-test. b) Controlled release by the reduction stimulus dithiothreitol (DTT). The time-dependent patterns of cumulative release of OSI-027 with (purple) or without (rose) DTT stimulus are illustrated with best-fit lines. *p < 0.001 for best-fit maximum cumulative release (R%), *vs.* DTT-free, extra sum-of-squares F test. c) Increased intracellular accumulation of OSI-027. Changed patterns of intracellular OSI-027 accumulation in Panc-02 cells treated with 5 μM (circle) or 10 μM (solid) of OSI-027 (orange) or MAP-mG3/OSI-027 (dark-blue) are shown. *p < 0.001, *vs.* 5 μM OSI-027, two-way ANOVA followed by Bonferroni's *post hoc* test. #p < 0.001, *vs.* 10 μM OSI-027, Bonferroni's test. ‡p < 0.05, ‡‡ p < 0.001, *vs.* 5 μM MAP-mG3, Bonferroni's test. d) Tumor accumulation *in vivo*. Representative photograph of distribution of Cy5 fluorescence in mice 2 h and 8 h after tail-vein injection of the Cy5-labelled nc-siRNA (Cy5-siRNA) or MAP-mG3/Cy5-siRNA system. e) *In vivo* OSI-027 distribution in the major organs and tumor tissues after intravenous MAP-mG3/OSI-027 or oral OSI-027 administration. * p < 0.001, Student's t test.

2.4. MAP-mG3/OSI-027 nanocapsules enhance therapeutic effect

To evaluate the therapeutic effect of MAP-mG3/OSI-027 on the mTOR pathway, we treated Panc-02 cells with nanoparticle-encapsulated OSI-027 or free OSI-027, and mTOR activation

(i.e., phosphorylated mTOR) was investigated by western blotting. An increased dose of MAP-mG3/OSI-027 and free OSI-027 led to increased inhibition of mTOR phosphorylation and downstream effectors such as p4E-BP1, and MAP-mG3/OSI-027 mediated similar [p-mTOR (Ser2481) with 64.4 ± 10.2 % expression decrease in 10μM MAP-mG3/OSI-027 treated cells *vs.* 76.9 ± 16.2 % in 10μM free OSI-027 treated cells; p = 0.493, paired t test] or more intense [p-mTOR (Ser2448), pAKT, and p4E-BP1] downregulation of the mTOR pathway compared with free OSI-027 (Fig. 4a). The mTOR pathway has been shown to be negatively associated with tumorigenesis and proliferation in various types of cancer, including pancreatic cancer[2, 24]. Motivated by the mTOR inhibitory effect of OSI-027 on Panc-02 cells, we investigated the effect of MAP-mG3/OSI-027 on proliferation of Panc-02 cells using cell-viability assays (Fig. 4b). A significantly enhanced anti-cancer effect compared with that for free OSI-027 treatment (best-fit half-maximal inhibitory concentration (IC_{50}), 7.4 ± 1.1 μM for MAP-mG3/OSI-027, and 14.9 ± 1.1 μM for free OSI-027, 95% CI; F = 54.9, p < 0.001, MAP-mG3/OSI-027 *vs.* free OSI-027, extra sum-of-squares F test) was noted. Accordingly, *in vitro* employment of the MAP-mG3/OSI-027 regimen enabled enhanced inhibition of mTOR expression and subsequent cancer-cell suppression, which allowed for further *in vivo* investigation against pancreatic cancer.

Next, we evaluated the therapeutic performance of MAP-mG3/OSI-027 nanocapsules in mice based on cancer growth after tail-vein administration in C57BL/6 mice bearing Panc-02 tumors (Fig. 4c, d), and was verified with positron emission tomography (Fig. 4e). In comparison with conventional oral treatment with OSI-027, MAP-mG3/OSI-027 administered *via* the intravenous route demonstrated a superior inhibitory effect on tumor growth *in vivo* starting after day-12 (p = 0.044, two-way ANOVA followed by Bonferroni's test; (n = 3) until mice sacrifice (p < 0.001; Bonferroni's test), with a final mean tumor volume of 243.7 ± 35.8 mm^3 and tumor weight of 0.3 ± 0.1 g as compared with a final mean tumor volume of 598.7 ± 72.4 mm^3 and final tumor weight of 1.2 ± 0.3 g for equivalent oral OSI-027 (p = 0.002 for volume and 0.005 for weight, Student's t-test, n = 3) (Fig. 4f, g). As expected, administration of the regular dose (25.0 mg/kg OSI-027 equivalent) showed a better therapeutic response than the half-dose regimen (12.5 mg/kg; final mean tumor volume and weight, 462.6 ± 46.8 mm^3 and 0.8 ± 0.2 g; n = 3; p = 0.003 for weight and 0.003 for volume, Student's t-test) 20 days after injection, suggesting a dose-dependent response in pancreatic cancer (Fig. 4f, g). MAP-mG3/OSI-027 was well tolerated during treatment without significant toxicity, though increased OSI-027 exposure was observed

in the major organs (Fig. S9 and Fig. 3e). Additional mechanistic studies revealed maximum attenuation of intratumoral expression of the proliferation indicator Ki67 (Fig. 4h) mediated by intravenous administration of MAP-mG3/OSI-027 among all the available treatment approaches. Comparison between dose-equivalent treatments confirmed the enhanced effect of MAP-mG3-encapsulated therapeutics, indicating the greater systemic exposure and efficacy of intravenous administration. Outcomes might benefit from an increased exposure dose of viable molecules, surpassing the scenario of limited dose and possible aggregation upon administration of insoluble agents.

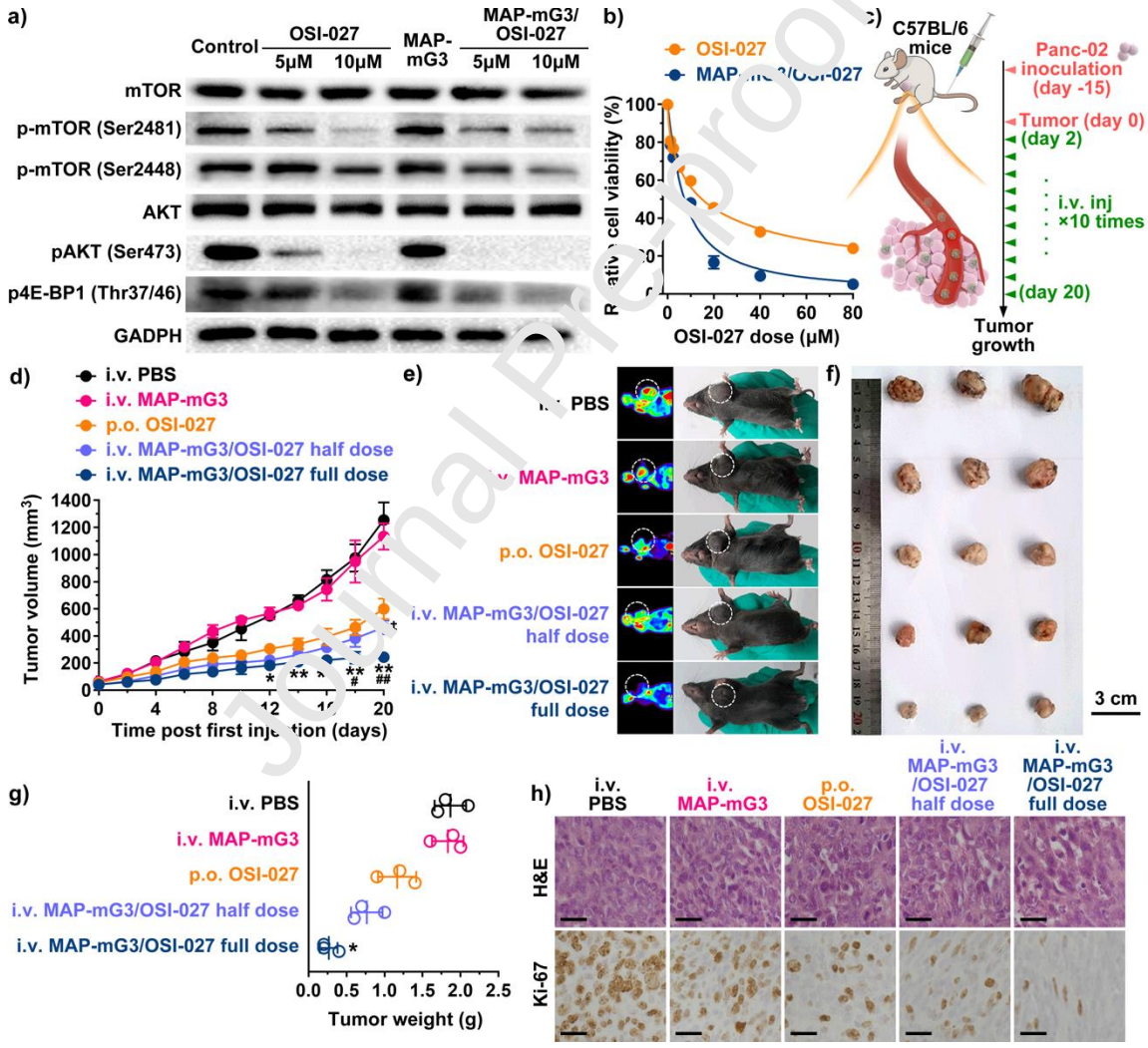

Figure 4. Biologic effect of the MAP-mG3/OSI-027 system on pancreatic cancer. a) Expression of total mTOR, phosphorylated mTOR (Ser2481 and Ser2448), total Akt, phosphorylated Akt (pAkt), and phosphorylated 4E-BP1 (p4E-BP1, Thr37/46) in Panc-02 cells treated with PBS (control), 5 μM or 10 μM of OSI-027 and MAP-mG3, or 5 μM or 10 μM of the MAP-mG3/OSI-

027 system by Western blotting. b) Dose-dependent toxicity of OSI-027 (orange) or equivalent MAP-mG3/OSI-027 (dark-blue) in Panc-02 cells, characterized by a cell-viability assay. Best-fit lines are shown. c) Drug administration (schematic) *in vivo*. p.o., *per ora*; i.v., intravenous. d) Tumor-growth patterns in mice treated with i.v. PBS (black), i.v. MAP-mG3 (rose), p.o. OSI-027 (orange), half-dose i.v. MAP-mG3/OSI-027 system (12.5mg/kg; light-purple), or full-dose i.v. MAP-mG3/OSI-027 system (25 mg/kg; dark-blue). *$p < 0.05$, **$p < 0.001$, *vs.* p.o. OSI-027, two-way ANOVA followed by Bonferroni's test. #$p < 0.001$, *vs.* p.o. OSI-027, Bonferroni's test. ‡$p < 0.01$, ‡‡$p < 0.001$, *vs.* half-dose MAP-mG3/OSI-027, Bonferroni's test. e) Representative positron emission tomography (PET) and white-field photographs of mice treated with indicated agents. Tumors are marked by white dashed circles. f) White-field photograph of tumors after treatment. The bar represents 3 cm. g) Comparison of tumor weights after treatment. *$p < 0.01$, *vs.* p.o. OSI-027, one-way ANOVA followed by Tukey's test. h) Representative pathology images and intratumoral Ki-67 expression in mice tumors after indicated treatment. The bar represents 20 μm.

2.5. MAP-mG3 system reverts OSI-027 chemoresistance

The decrease in the dose-related change in response by MAP-mG3/OSI-027 offered insights into the drug viability and possible drug resistance involved. Drug resistance (especially resistance to targeted agents) is a serious problem that develops frequently in patients treated long-term with targeted agents[25]. To explore new strategies against drug resistance, an OSI-027-resistant Panc-02 cell line (Panc-02/DR) was established (best-fit $IC_{50} = 48.0 \pm 9.0$ μM, 95% CI; $F = 238.1$, $p < 0.001$, *vs.* regular Panc-02, extra sum-of-squares F test) (Fig. 5a) with markedly altered gene expression (particularly in transporter systems) in biological process classification analysis for the 50 most significant differentially expressed genes using high-throughput RNA sequencing microarrays (Fig. S10). To ascertain whether MAP-mG3 could restore the biologic effect of OSI-027 in resistant Panc-02 cells, anti-cancer activity *in vitro* was measured. We showed sharp discrimination in inhibition of proliferation of Panc-02/DR cells between MAP-mG3/OSI-027 treatments ($IC_{50} = 8.3 \pm 1.0$ μM, 95% CI) and free OSI-027 ($F = 268.7$, $p < 0.001$, extra sum-of-squares F test) (Fig. 5a). Notably, no difference in cytotoxicity was observed between Panc-02 and Panc-02/DR cells treated with MAP-mG3/OSI-027 ($F = 1.8$, $p = 0.189$, extra sum-of-squares F test). These results suggested that MAP-mG3/OSI-027 could overcome OSI-027 resistance in Panc-02/DR cells *in vitro*. Meanwhile, 3.58-fold enhancement of OSI-027 accumulation was demonstrated in Panc-02/DR cells incubated with MAP-mG3/OSI-027 (4.4 ± 0.2 μg/mg protein) ($n = 3$) in comparison with free OSI-027 (1.2 ± 0.2

μg/mg protein) (n = 3, $p < 0.001$, Student's t-test) (Fig. 5b), indicating the excellent internalization facilitated by MAP-mG3 to be a major contributory factor for OSI-027 sensitization. Increasing numbers of studies have shown that nanocapsules can reverse drug resistance in stressed or resistance-induced cells by improving internalization and subsequent drug viability[26-28], in accordance with the reversed resistance observed in our study.

To validate anti-drug resistance *in vivo*, we applied MAP-mG3/OSI-027 systemically to mice bearing xenograft Panc-02/DR tumors. Drug-resistant tumor growth showed a remarkable inhibitory pattern mediated by MAP-mG3/OSI-027 administration as compared with OSI-027 or control (phosphate-buffered saline, PBS) given *via* the oral route ($p < 0.001$, *vs.* MAP-mG3/OSI-027, two-way ANOVA followed by Bonferroni's test) (Fig. 5c). Clearly, MAP-mG3/OSI-027 outperformed the free drug in reducing tumor volume (final mean tumor volume and weight, 273.8 ± 40.7 mm^3 and 0.3 ± 0.1 g for MAP-mG3/OSI-027, 971.7 ± 126.2 mm^3 and 1.5 ± 0.2 g for OSI-027; n = 3; $p < 0.001$, Student's t-test), which resulted in increased reversal of drug resistance (Fig. 5d). Thus, MAP-mG3 substantially restored OSI-027 sensitivity to drug resistance *in vivo*, which suggested the application potential of MAP-mG3 encapsulation to overcome resistance. This sensitivity restoration could permit prolonged targeted therapy (which could be associated with increased survival) and reduce unnecessary dose escalation (which might allow better tolerance in various clinical settings)[29-31].

To explore the mechanism of MAP-mG3/OSI-027 in regulating chemoresistance in Panc-02/DR cells, we further compared the expression change of mTOR-related pathways and resistance pathways by RNA sequencing microarrays (Fig. 5e, f). A wide range of downstream pathways and compensatory pathways, including Akt, Sqle, Seme7a, and Erk1/2, were significantly regulated by MAP-mG3/OSI-027 in comparison to free OSI-027 (Fig. 5g), confirming the effective mTOR inhibition of the nanocapsules in drug-resistant cells. The OSI-027 resistance might cause ineffective mTORC2 inhibition, which, together with other compensatory activation pathways, would contribute to abnormal Erk1/2 upregulation[32, 33]. Meanwhile, the resistance pathways, specifically the ATP-binding cassette (ABC) transporter family, were also significantly altered by MAP-mG3/OSI-027 treatment. Notably, Abcb1 (including both Abcb1a and Abcb1b) expression was high in resistant cells and slightly upregulated after OSI-027 treatment, and was attenuated by MAP-mG3/OSI-027 treatment, but

not by the MAP-mG3 vector, verified by immunoblotting (Fig. 5g and Fig. S11). Combination administration of tariquidar, a P-gp inhibitor to block ABCB1 and MDR, with free OSI-027 treatment, resulted in a significantly enhanced antiproliferation effect in OSI-027-resistant cells, but less effective than MAP-mG3/OSI-027 (Fig. 5h). Notably, ABCB1 overexpression could still hinder the effect of resistance reversal by MAP-mG3/OSI-027. These data suggest that MAP-mG3 nanocapsules regulate OSI-027 chemoresistance by inhibiting ABC-associated resistance pathways as well as compensatory pathways.

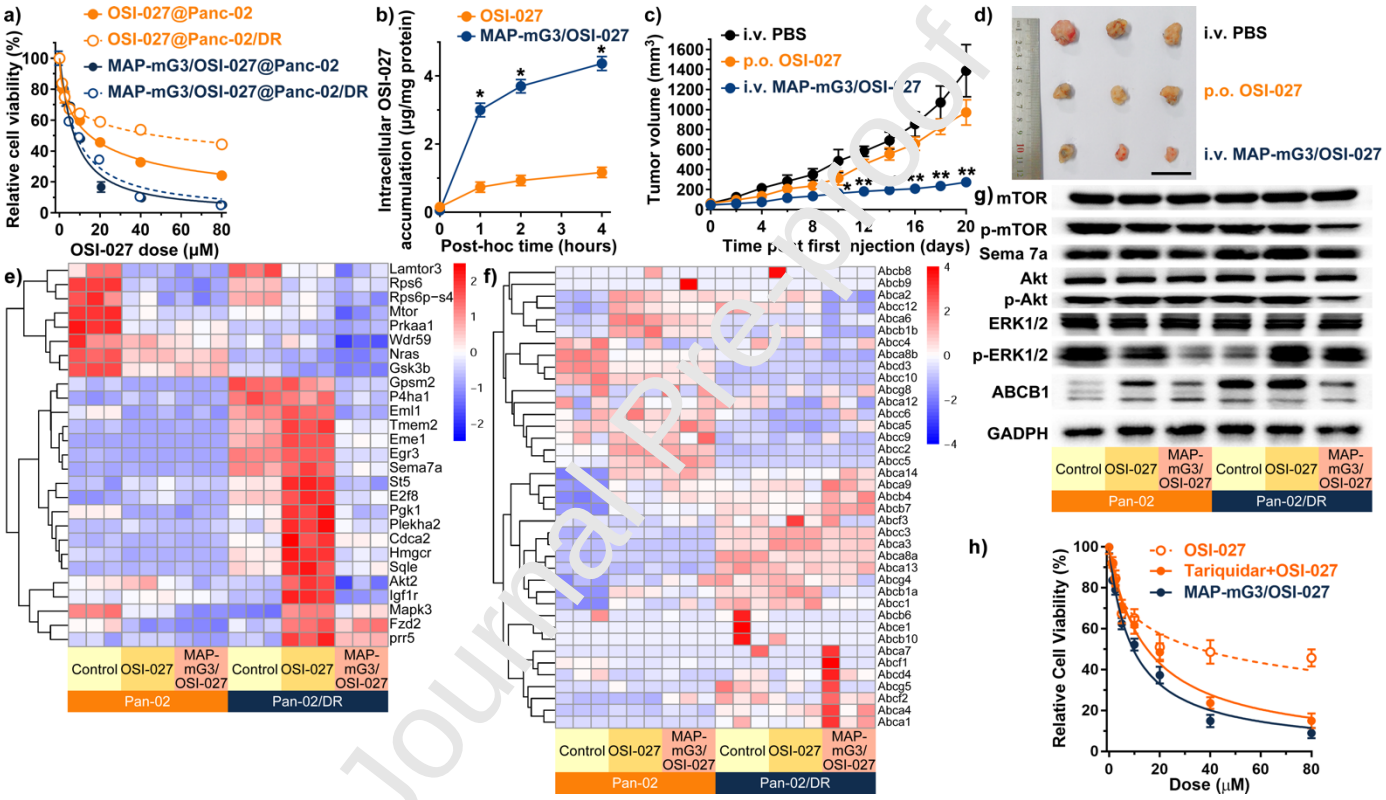

Figure 5. Reversal of OSI-027 chemoresistance by the MAP-mG3 system. a) Establishment of OSI-027-resistant Panc-02 cells (Panc-02/DR). Dose-dependent cytotoxicity of OSI-027 (orange) and equivalent MAP-mG3/OSI-027 (dark-blue) in regular Panc-02 cells (solid) or drug-resistant Panc-02/DR cells (circle), characterized by a cell-viability assay. Best-fit lines for Panc-02 cells (solid) and Panc-02/DR cells (dashed) are shown. b) Increased intracellular accumulation of OSI-027 in Panc-02/DR cells. *p < 0.001, *vs.* OSI-027, two-way ANOVA followed by Bonferroni's test. c) Tumor-growth patterns in mice treated with i.v. PBS (black), p.o. OSI-027 (orange), or i.v. MAP-mG3/OSI-027 system (dark blue). *p < 0.05, **p < 0.001, *vs.* p.o. OSI-027, Bonferroni's test. d) White-field photograph of Panc-02/DR tumors after treatment. The bar represents 3 cm. e, f) Hierarchical clustering of gene expression data for mTOR-related pathways and ABC family among treatment with control, free OSI-027, or MAP-

mG3/OSI-027 in Panc-02 and Panc-02/DR cells. The bars represent expression change fold. g) Expression of total mTOR, phosphorylated mTOR, sema7a, total Akt, phosphorylated Akt, total Erk1/2, and Erk1/2 in mTOR-related pathways and ABCB1 in Panc-02 and Panc-02/DR cells treated with control, free OSI-027, or MAP-mG3/OSI-027. h) Dose-dependent toxicity of OSI-027 (orange circle), OSI-027 and tariquidar combination (orange solid), or MAP-mG3/OSI-027 in Panc-02/DR cells (dark-blue solid), characterized by a cell-viability assay. Best-fit lines are shown.

3. Discussions

Unlike MAP-pG2 or MAP-pG3, MAP-mG2 and MAP-mG3 can load considerable amounts of hydrophobic therapeutic agents while retaining acceptable solubility for intravenous applications. The underlying mechanism of enhanced drug loading in MAP-mG2 and MAP-mG3 might be associated with co-delivered nucleotides and the difference in the molecular structures of the dendrimers. The most remarkable difference between the PAMAM dendrimers (pG2 and pG3) and modified dendrimers (mG2 and mG3) should be the allocation of cationic charges provided mostly by amine groups. That is, the modified dendrimers, with a pentaerythritol core and inner ether bonds, have cationic amine charges located mainly at the outer surface whereas the PAMAM dendrimers, with an ethylenediamine core and inner quaternary ammonium linkages, have a nearly uniform distribution of cationic charges. When condensing nucleotides, the modified dendrimers can form a "blocking shell" with a cationic outer layer to reinforce capsulation, which cannot be accomplished with the PAMAM dendrimers. A similar mechanism could also explain the superior loading capacity of MAP-mG3 in comparison with MAP-mG2 because the inner space of MAP-mG3 within the blocking shell should be greater based on reported or simulated structure models[34]. There are other possible mechanisms, including the hydrophobic inner structures of ether bonds and outer shell density of the amine groups in the modified dendrimers, contributing to the increase in loading capacity, supported by lower inhibition constant in the simulated drug–dendrimer interference model.

A close analog to the MAP-mG3/OSI-027 system is the PEGylated OSI-027 complex (PEG-OSI-027). PEG/OSI-027 or MAP-mG3/OSI-027 features have satisfactory solubility due to shared PEG components, but MAP-mG3 outperforms the PEGylated complex in three important ways. First, MAP-mG3 provides sufficient vacancies for multiple drug molecules whereas the

linear structure of regular PEG limits them. Second, MAP-mG3 allows for drug encapsulation by non-covalent interactions, but regular PEGylation requires covalent linkage between the drug and PEG chain, which could hinder release significantly. Finally, MAP-mG3 possesses the advantage of functional delivery due to designed controlled release, which the regular PEGylated complex does not. The PEGylated complex has evolved continually to develop new features, such as responsive linkage between the drug and PEG[35], but cannot reverse the disadvantages mentioned above simultaneously.

The superior features of the MAP-mG3 system expedited intravenous use of targeted agents in preclinical studies, circumventing the first-pass effect *via* oral administration and metabolism of cytochrome enzymes[36]. We have proposed the potential of an intravenous approach with polymer inclusion of the tyrosine kinase inhibitor gefitinib, and showed enhancement in the therapeutic effect[10]. The present study substantiated the hypothesis that introduction of the MAP-mG3 system (rather than our previous inclusion of a non-functional polymer) could facilitate chemoresistance reversal by multiple mechanisms, enabling engineered reuse of resistant targeted agents. Our results suggest the possibility of intravenous administration (rather than oral administration) of targeted agents with the aid of an appropriately designed delivery system to overcome chemoresistance in previously resistant individuals.

4. Conclusions

In summary, we developed the MAP-mG3 delivery system optimized for functional delivery of a targeted agent against pancreatic cancer. This system enables water solubility of hydrophobic drugs and increases dose exposure at the tumor site, leading to reversal of developed drug resistance. MAP-mG3 could be adapted further as a potentially safe and efficient delivery system for other targeted therapeutics in future biomedical and preclinical applications against malignancies.

5. Materials and methods

5.1. *Materials*

OSI-027 and tariquidar was purchased from Selleck Chemicals (Houston, TX). 1,4-butanediamine, cystamine dihydrochloride, NHS-PEG-OH (molecular weight (MW) = 2000 Da), eight-armed PEG (bPEG, MW = 15000 Da), trimethylamine (NEt_3), 1,1'- carbonyldiimidazole (CDI), dithiothreitol (DTT), 3-(4,5-dimethylthiazol-2-yl)-2,5-diphenyltetrazolium bromide (MTT) were purchased from Sigma-Aldrich (Saint Louis, MO). Poly(amidoamine) dendrimers (PAMAM) second-generation G2 (pG2) and PAMAM third-generation G3 (pG3) were purchased from Dendritech (Midland, MI). 2-(4-amidinophenyl)-6-indolecarbamidine dihydrochloride (DAPI) was obtained from Beyotime Biotechnology (Haimen, China). 1-(3-dimethylaminopropyl)-3-ethylcarbodiimide hydrochloride (EDC·HCl), 4-(dimethylamino)-pyridine (DMAP) and fluorescein isothiocyanate (FITC) were purchased from Aladdin Industrial (Shanghai, China). Dialysis membranes were obtained from Spectrum Laboratories (Rancho Dominguez, CA). Fluorescence-tagged negative-control small interfering (si)RNA (FITC-siRNA and Cy5.5-siRNA) was purchased from Biomics Biotechnologies (Nantong, China).

5.2. *Cell*

Mouse pancreatic cancer Panc-02 cell lines were purchased from American Type Culture Collection (Rockville, MD) and cultured in Dulbecco's modified Eagle's medium (DMEM) containing 10% fetal bovine serum (FBS). Cells were grown under humidified air containing 5% CO_2 at 37 °C.

5.3. *Synthesis of bPEG-SS-PEG-mG2 (MAP-mG2), bPEG-SS-PEG-mG3 (MAP-mG3), bPEG-SS-PEG-PAMAM G2 (MAP-pG2), bPEG-SS-PEG-PAMAM G3(MAP-pG3)*

bPEG-SS-PEG (2 g, 0.12 mmol) dissolved in DMSO (10 mL) was added to a solution of CDI (2 g, 12 mmol) and Et_3N (2 mL, 14.4 mmol) in DMSO (10 mL) at room temperature. The reaction mixture was stirred for 5 h. After that, the resulted product was precipitated in 1 L of ether/THF solution (v:v = 4:1) and was redissolved in DMSO (10 mL), which was subsequently added dropwise to pG2 dendrimer (4 g, 0.72 mmol), pG3 dendrimer, mG2 dendrimer and mG3 dendrimer in DMSO solution (10 mL) in the presence of triethylamine (300 μL, 2.9 mmol). After being stirred for 12 h, the final product was purified by extensive dialysis against water using

molecular weight cutoff (MWCO) = 14,000 dialysis membrane and was freeze-dried to yield the final product MAP-pG2, MAP-pG3, MAP-mG2 and MAP-mG3.

5.4. Preparation of MAP-pG2/OSI-027, MAP-pG3/OSI-027, MAP-mG2/OSI-027 and MAP-mG3/OSI-027 complexes and determination of loading capacity

OSI-027 (10.0 mg) was dissolved in dimethyl sulfoxide (DMSO) (2 mL). MAP-pG2, MAP-pG3, MAP-mG2 and MAP-mG3 (40.0 mg) were dissolved in water (10 mL). After both substances had dissolved completely, the two solutions were mixed, and the mixture stirred overnight. The solution was purified by dialysis against water and DMSO using a dialysis membrane (MWCO = 14,000) for 12 h. Then, the solution was passed through a 0.45-mm filter to remove the unloaded OSI-027 and lyophilized to afford a faint-yellow powder (MAP-pG2/OSI-027, MAP-pG3/OSI-027, MAP-mG2/OSI-027 and MAP-mG3/OSI-027). The drug-loading content was measured by an Ultraviolet–visible spectroscopy or ultraviolet-visible (UV-vis) spectrophotometry (UV-2800, Hitachi, Tokyo, Japan). Then, 4.0 mg of freeze-dried MAP-pG2/OSI-027, MAP-pG3/OSI-027, MAP-mG2/OSI-027 and MAP-mG3/OSI-027 nanoparticles were dissolved in 20 mL of water and absorbance measured at λ = 342 nm. A calibration curve was established under identical conditions. The drug loading content of MAP-pG2/OSI-027, MAP-pG3/OSI-027, MAP-mG2/OSI-027 and MAP-mG3/OSI-027 micelles for OSI-027 was calculated using the following formula: Loading % = mass of OSI-027 encapsulated in micelles/mass of micelles × 100%.

5.5. K_i calculation for p-G2/OSI-027, p-G2/OSI-027, p-G2/OSI-027 and p-G2/OSI-027

The protein date bank (PDB) files of OSI-027 and different dendrimers (pG2, pG3, mG2 and mG3) were optimized geometrically using the energy minimization method via Chemical Bio3D Ultra (Perkin Elmer, 14.0.0.117). Then, the AutoDock Tools package and AutoDock Vina (Scripps Research Institute, La Jolla, USA) were employed to conduct docking studies. In docking simulation, OSI-027 was used as a ligand, whereas dendrimers (pG2, pG3, mG2 and mG3) were used as receptors. Gasteiger charges were computed for each of the molecules. Grid maps were prepared using a 100 × 100 × 100 grid box with the distance between two grid points set at 0.375 Å centered on each dendrimer (pG2, pG3, mG2 and mG3). All rotational bonds of OSI-027 were set free, whereas those of the dendrimer were held rigid. Docking studies were

carried out using the "empirical free energy function" and applying the standard protocol of the Lamarckian Genetic Algorithm. Five-hundred independent docking runs were carried out for each docking process with a maximum number of 27,000 generations, a mutation rate of 0.02, a crossover rate of 0.8, and an elitism value of 1. All other parameters were the default values by AutoDock Vina. The docking pose with the highest score was treated as the stable binding model. The docking score from the AutoDock Vina output was used as the binding free energy. According to docking results, the minimum binding energies between OSI-027 and dendrimers (pG2, pG3, mG2 and mG3) were −8.91, −10.41, −11.72 and −17.99 kcal/mol, and the inhib_constant (K_i) was 985.6 nM, 23.22 nM, 2.58 nM and 65.48 fM, respectively. Inhib_constant was calculated in AutoDock as:

$$K_i = \exp(\Delta G \times 1000)/(Rcal \times TK) \quad (1)$$

Where ΔG is the docking energy, Rcal is 1.98719 and TK is 298.15.

5.6. Solubility measurement of OSI-027 and MAP-mG3/OSI-027

Excessive MAP-mG3/OSI-027 or OSI-027 was added in Eppendorf tubes with 5 mL of H_2O, respectively. These tubes were stirred at 100 rpm for 24 h on an orbital shaker at 37 °C. Then, the saturated supernatant and undissolved powder were obtained by filtering through a syringe filter (0.45 μm, Whatman, Little Chalfont, UK). The saturation concentration was determined by UV-Vis spectrometry at λ = 342 nm using 2 mL of supernatant removed accurately from the tubes.

5.7. In vitro release behavior of MAP-mG3/OSI-027/siRNA

First, 5.0 mg of MAP-mG3/OSI-027/siRNA was dissolved in 10 mL of PBS at pH = 7.4 and sealed in dialysis tubing (MWCO = 8,000–14,000). The solution was dialyzed against 45 mL of PBS in the absence or presence of 10 mM of DTT at 37 °C under stirring at 87 rpm on an orbital shaker. At defined time points, 1 mL of the medium was removed from the 45-mL solution out of the dialysis bag for HPLC and was then returned to the original system. The amount of OSI-027 released was measured by HPLC at a maximum absorption wavelength of 342 nm.

5.8. Establishment of OSI-027-resistant cell lines and a mice xenograft model

OSI-027 resistant Panc-02 cells (Panc-02/DR) were transformed from regular Panc-02 cells by induction using low-dose OSI-027, starting from 0.5 μM and increasing stepwise to 10 μM. Eventually after 5 months of induction, OSI-027-resistant cells with a resistance index (RI) of 3.2 were obtained. The mice xenograft model was established in female C57BL/6 mice of age 4–6 weeks bred under standard pathogen-free conditions. Each mouse was injected subcutaneous in the subaxillary flank with 1×10^6 Panc-02 or Panc-02/DR cells suspended in 150 μL of PBS. When the xenograft tumor volume reached 50–70 mm^3, tumor-bearing mice were treated with the indicated regimen *via* tail-vein administration.

5.9. HPLC assay

HPLC method was used for determining the concentration of OSI-027. The analytical column was a Agilent Eclipse-XDB-C18 column (4.6 mm × 250 mm, 5 μm). The mobile phase was CH_3CN: H_2O (35 : 65 v/v), the flow rate of mobile phase was 0.7 mL min^{-1} and the UV detector was at 342 nm.

5.10. Determination of intracellular accumulation dose

The intracellular drug concentration of free OSI-027, MAP-mG3/OSI-027 in Panc-02 or Panc-02/DR cells was measured by HPLC from cell lysates. Briefly, pre-seeded cells were treated with different OSI-027 formulations for 1, 2, or 4 h at 37 ºC. After incubation, cells were collected, washed thrice with cold PBS, and lysed with 1% Triton X-100. Protein content and OSI-027 concentration in the cell lysate were detected by bicinchoninic acid protein assay and HPLC, respectively, which determined the OSI-027 concentration normalized by the total protein content.

5.11. Serum stability of MAP-mG3 system

For hemolytic studies, the red blood cell (RBC) suspension was dispersed in distilled water and PBS buffer. Distilled water was considered as 100% hemolytic, and PBS buffer as non-hemolytic as control. A series concentration of MAP-mG3/OSI-027/siRNA were added to a 2% w/v solution of freshly prepared sheep red blood cells in PBS buffer and incubated for 1 h at 37°C in a shaking water bath. The samples were centrifuged (1500 g for 10 min) and the supernatants were assayed spectrophotometrically for the presence of free hemoglobin (λ= 540

nm). As for the time-dependent size pattern of MAP-mG3/OSI-027/siRNA (100 μg/mL in PBS buffer and serum-containing solution) was measured at a predetermined time point.

5.12. In vivo pharmacokinetic and distribution study

In vivo pharmacokinetic and distribution study of OSI-027 (from free OSI-027 and MAP-mG3/OSI-027) in heart, liver, spleen, lung, kidneys and tumor were carried out via oral administration and intravenous administration with dose 25 mg/kg OSI-027. OSI-027 concentration was determined by HPLC systems.

5.13. Cytotoxicity assay

Panc-02 and Panc-02/DR cells were seeded in 96-well plates at 8000 cells/well in 200 μL of DMEM containing with 10% FBS for 18 h. Subsequently, the cells were incubated with culture medium containing MAP-mG3/OSI-027/siRNA, MAP-mG3/siRNA and OSI-027 with different concentrations for 72 h. As for tariquidar + OSI-027 test, a 2μM tariquidar and OSI-027 with different concentrations was utilize. Then, 100 μl of DMEM containing MTT stock solution (1 mg/mL) was added to the wells. After incubation for another 4 h, each well was replaced with 100 μL of DMSO. The absorbance was measured at 570 nm using an ELISA plate reader (Model 550, Bio-Rad, Hercules, CA). The relative cell growth (%) related to control cells cultured in the media without the polymer was calculated by the following formula:

$$V\% = \frac{([A]\text{experimental} - [A]\text{blank})}{([A]\text{control} - [A]\text{blank})} \times 100\% \quad (2)$$

Where V% is the relative cell viability (%), [A]experimental is the absorbance of the wells culturing the treated cells, [A]blank is the absorbance of the blank, and [A]control is the absorbance of the wells culturing untreated cells.

5.14. Determine the expression of phosphor-mTOR pathway protein

Panc-02 cells were seeded into 6-well plates at a density of 2×10^5 cells per well and incubated for 18 h. Cells were then treated with free OSI-027 (5 μM, 10 μM) and MAP-mG3/OSI-027 (5 μM, 10 μM) for 72 h, washed with ice-cold PBS and harvested in 100 μL cell lysis buffer (Cell Signaling, Danvers, MA) containing protease inhibitors (Sigma-Aldrich, Saint Louis, MO)). The protein concentration of lysates was determined using the bicinchoninic acid

method (Thermo, Rockford, IL). Cell lysate samples (30 μg per lane) were separated using 10% SDS-PAGE and transferred electrophoretically to polyvinylidene difluoride mem-branes (Millipore, Billerica, MA). Membranes were blocked with Tris-buffered saline/0.1% Tween 20 (TBS/T) containing 5% bovine serum albumin (BSA) and incubated overnight at 4 °C with anti-phospho-mTOR (Ser2481), anti-phospho-mTOR (Ser2448), anti-phospho-Akt (Ser473) and anti-phospho-4E-BP1 (Thr37/46) (1:1000; Cell Signaling, Danvers, MA). Membranes were washed three times with TBS/T and incubated for 1 h at room temperature with the appropriate secondary antibody conjugated to goat anti-mouse horseradish peroxidase (Cell Signaling, Danvers, MA) (1:2000; GE Healthcare, Piscataway, NJ). Membranes were then washed and immunoreactive bands were developed using an enhanced chemiluminescence reagent and visualized by autoradiography. Protein loading was normalized using an anti-GAPDH antibody (Proteintech Group Wuhan, China) (1:5000, Kangchen Biotechnology, Shanghai, China). Gray-scale analysis of protein bands was performed using ImageJ software (National Institutes of Health, Bethesda, MD).

5.15. In vivo therapeutic study

For the tumor suppression study, the mice were randomly divided into five groups (n = 3 per group). The mice bearing Panc-02 tumors were treated with PBS, MAP-mG3, free OSI-027 (oral, 25 mg/kg), MAP-mG3/OSI-027 (i.v. 25.0 mg/kg OSI-027 equivalent for full dose, 12.5 mg/kg for half dose). The mice received injections on days 15 after tumor cell implantation. Treatment (oral or intravenous administration) was performed every two days for 10 times. Tumor growth was monitored by measuring the perpendicular diameter of the tumor using calipers. Tumor volume (mm^3) was calculated as:

$$v = \frac{l \times w^2}{2} \quad (3)$$

in which l and w indicate the length and width of the tumor.

5.16. Quantification of gene expression level

Feature Counts v1.5.0-p3 was used to count the reads numbers mapped to each gene. And then (Fragments Per Kilobase of transcript per Million fragments mapped) FPKM of each gene was calculated based on the length of the gene and reads count mapped to this gene. FPKM, expected

number of FPKM base pairs sequenced, considers the effect of sequencing depth and gene length for the reads count at the same time, and is currently the most commonly used method for estimating gene expression levels.

5.17. Differential expression analysis

Differential expression analysis of two conditions/groups (two biological replicates per condition) was performed using the DESeq2 R package (1.16.1). DESeq2 provide statistical routines for determining differential expression in digital gene expression data using a model based on the negative binomial distribution. The resulting P-values were adjusted using the Benjamini and Hochberg's approach for controlling the false discovery rate. Genes with an adjusted P-value <0.05 found by DESeq2 were assigned as differentially expressed. The false discovery rate was set to be <0.05.

5.18. Statistical analyses

Experiments were repeated at least thrice. Data are the mean ± SD. Statistical calculations were made using Prism 7 (GraphPad, La Jolla, CA) with the indicated analytical methods. Data from nuclear magnetic resonance were analyzed by Mestrelab Research (Santiago de Compostela, Spain), and flow-cytometry data were analyzed using FlowJo 10 (FlowJo, Ashland, OR). Best-fit values and 95% confidence intervals (CIs) were calculated using indicated nonlinear regression. $p < 0.05$ was considered significant.

Acknowledgements

This work was supported financially by the National High Technology Research and Development Program 863 of China (SS2015AA020405), the National Natural Science Foundation of China (81502026, 81830089, and 81530079) and Zhejiang Provincial Natural Science Foundation (LQ16H180002 and LY18H160026).

Appendix A. Supplementary data

Supplementary data related to this article can be found at

References

[1] C.L. Wolfgang, J.M. Herman, D.A. Laheru, A.P. Klein, M.A. Erdek, E.K. Fishman, R.H. Hruban, Recent progress in pancreatic cancer, CA Cancer J Clin, 63 (2013) 318-348.

[2] X. Zhi, W. Chen, F. Xue, C. Liang, B.W. Chen, Y. Zhou, L. Wen, L. Hu, J. Shen, X. Bai, T. Liang, OSI-027 inhibits pancreatic ductal adenocarcinoma cell proliferation and enhances the therapeutic effect of gemcitabine both in vitro and in vivo, Oncotarget, 6 (2015) 26230-26241.

[3] M.M. Javle, R.T. Shroff, H. Xiong, G.A. Varadhachary, D. Fogelman, S.A. Reddy, D. Davis, Y. Zhang, R.A. Wolff, J.L. Abbruzzese, Inhibition of the mammalian target of rapamycin (mTOR) in advanced pancreatic cancer: results of two phase II studies, BMC Cancer, 10 (2010) 368.

[4] B.M. Wolpin, A.F. Hezel, T. Abrams, L.S. Blaszkowsky, J.A. Meyerhardt, J.A. Chan, P.C. Enzinger, B. Allen, J.W. Clark, D.P. Ryan, C.S. Fuchs, Oral mTOR inhibitor everolimus in patients with gemcitabine-refractory metastatic pancreatic cancer, J Clin Oncol, 27 (2009) 193-198.

[5] C.G. Da Silva, G.J. Peters, F. Ossendorp, J.J. Cruz, The potential of multi-compound nanoparticles to bypass drug resistance in cancer, Cancer Chemother Pharmacol, 80 (2017) 881-894.

[6] T. Muranen, L.M. Selfors, D.T. Worster, M.P. Iwanicki, L. Song, F.C. Morales, S. Gao, G.B. Mills, J.S. Brugge, Inhibition of PI3K/mTOR leads to adaptive resistance in matrix-attached cancer cells, Cancer Cell, 21 (2012) 227-239.

[7] J. Shen, Q. Wang, Q. Hu, Y. Li, G. Tang, P.K. Chu, Restoration of chemosensitivity by multifunctional micelles mediated by P-gp siRNA to reverse MDR, Biomaterials, 35 (2014) 8621-8634.

[8] D.D. Von Hoff, T. Ervin, F.P. Arena, E.G. Chiorean, J. Infante, M. Moore, T. Seay, S.A. Tjulandin, W.W. Ma, M.N. Saleh, M. Harris, M. Reni, S. Dowden, D. Laheru, N. Bahary, R.K. Ramanathan, J. Tabernero, M. Hidalgo, D. Goldstein, E. Van Cutsem, X. Wei, J. Iglesias, M.F. Renschler, Increased survival in pancreatic cancer with nab-paclitaxel plus gemcitabine, N Engl J Med, 369 (2013) 1691-1703.

[9] J.H. Moon, J.W. Moxley, Jr., P. Zhang, H. Cui, Nanoparticle approaches to combating drug resistance, Future Med Chem, 7 (2015) 1503-1510.

[10] K. Wang, Q.D. Hu, W. Zhu, M.M. Zhao, Y. Ping, G.P. Tang, Structure-Invertible Nanoparticles for Triggered Co-Delivery of Nucleic Acids and Hydrophobic Drugs for Combination Cancer Therapy, Adv Funct Mater, 25 (2015) 3380-3392.

[11] Y. Cheng, L. Zhao, Y. Li, T. Xu, Design of biocompatible dendrimers for cancer diagnosis and therapy: current status and future perspectives, Chem Soc Rev, 40 (2011) 2673-2703.

[12] J.F. Kukowska-Latallo, A.U. Bielinska, J. Johnson, R. Spindler, D.A. Tomalia, J.R. Baker, Jr., Efficient transfer of genetic material into mammalian cells using Starburst polyamidoamine dendrimers, Proc Natl Acad Sci U S A, 93 (1996) 4897-4902.

[13] Q. Xu, C.H. Wang, D.W. Pack, Polymeric carriers for gene delivery: chitosan and poly(amidoamine) dendrimers, Curr Pharm Des, 16 (2010) 2350-2368.

[14] Y. Cheng, Y. Li, Q. Wu, J. Zhang, T. Xu, Generation-dependent encapsulation/electrostatic attachment of phenobarbital molecules by poly(amidoamine) dendrimers: Evidence from 2D-NOESY investigations, Eur J Med Chem, 44 (2009) 2219-2223.

[15] G. Macnab, J.S. Harington, Haemolytic activity of asbestos and other mineral dusts, Nature, 214 (1967) 522-523.

[16] S.V. Bhagwat, P.C. Gokhale, A.P. Crew, A. Cooke, Y. Yao, C. Mantis, J. Kahler, J. Workman, M. Bittner, L. Dudkin, D.M. Epstein, N.W. Gibson, R. Wild, L.D. Arnold, P.J. Houghton, J.A. Pachter, Preclinical characterization of OSI-027, a potent and selective inhibitor of mTORC1 and mTORC2: distinct from rapamycin, Mol Cancer Ther, 10 (2011) 1394-1406.

[17] J. Mateo, D. Olmos, H. Dumez, S. Poondru, N.L. Samberg, S. Barr, J.M. Van Tornout, F. Jie, S. Sandhu, D.S. Tan, V. Moreno, P.M. LoRusso, S.B. Kaye, P. Schoffski, A first in man, dose-finding study of the mTORC1/mTORC2 inhibitor OSI-027 in patients with advanced solid malignancies, Br J Cancer, 114 (2016) 889-896.

[18] T. Schnelldorfer, S. Gansauge, F. Gansauge, S. Schlosser, H.G. Beger, A.K. Nussler, Glutathione depletion causes cell growth inhibition and enhanced apoptosis in pancreatic cancer cells, Cancer, 89 (2000) 1440-1447.

[19] Q. Hu, K. Wang, X. Sun, Y. Li, Q. Fu, T. Liang, G. Tang, A redox-sensitive, oligopeptide-guided, self-assembling, and efficiency-enhanced (ROSE) system for functional delivery of microRNA therapeutics for treatment of hepatocellular carcinoma, Biomaterials, 104 (2016) 192-200.

[20] Y. Patil, T. Sadhukha, L. Ma, J. Panyam, Nanoparticle-mediated simultaneous and targeted delivery of paclitaxel and tariquidar overcomes tumor drug resistance, J Control Release, 136 (2009) 21-29.

[21] M.M. Gottesman, Mechanisms of cancer drug resistance, Annu Rev Med, 53 (2002) 615-627.

[22] H. Maeda, H. Nakamura, J. Fang, The EPR effect for macromolecular drug delivery to solid tumors: Improvement of tumor uptake, lowering of systemic toxicity, and distinct tumor imaging in vivo, Adv Drug Deliv Rev, 65 (2013) 71-79.

[23] T. Sun, Y.S. Zhang, B. Pang, D.C. Hyun, M. Yang, Y. Xia, Engineered nanoparticles for drug delivery in cancer therapy, Angew Chem Int Ed Engl, 53 (2014) 12320-12364.

[24] Y. Guri, M. Colombi, E. Dazert, S.K. Hindupur, J. Roszik, S. Moes, P. Jenoe, M.H. Heim, I. Riezman, H. Riezman, M.N. Hall, mTORC2 Promotes Tumorigenesis via Lipid Synthesis, Cancer Cell, 32 (2017) 807-823 e812.

[25] J. Mattern, Drug resistance in cancer: a multifactorial problem, Anticancer Res, 23 (2003) 1769-1772.

[26] J.L. Markman, A. Rekechenetskiy, E. Holler, J.Y. Ljubimova, Nanomedicine therapeutic approaches to overcome cancer drug resistance, Adv Drug Deliv Rev, 65 (2013) 1866-1879.

[27] M. Susa, A.K. Iyer, K. Ryu, F.J. Hornicek, H. Mankin, M.M. Amiji, Z. Duan, Doxorubicin loaded Polymeric Nanoparticulate Delivery System to overcome drug resistance in osteosarcoma, BMC Cancer, 9 (2009) 399.

[28] Y.Y. Xu, Y.Z. Du, H. Yuan, L.N. Liu, Y.P. Niu, F.Q. Hu, Improved cytotoxicity and multidrug resistance reversal of chitosan based polymeric micelles encapsulating oxaliplatin, J Drug Target, 19 (2011) 344-353.

[29] A. Shapira, Y.D. Livney, H.J. Broxterman, Y.G. Assaraf, Nanomedicine for targeted cancer therapy: towards the overcoming of drug resistance, Drug Resist Updat, 14 (2011) 150-163.

[30] X.Z. Yang, X.J. Du, Y. Liu, Y.H. Zhu, Y.Z. Liu, Y.P. Li, J. Wang, Rational Design of Polyion Complex Nanoparticles to Overcome Cisplatin Resistance in Cancer Therapy, Adv Mater, 26 (2014) 931-936.

[31] M.Z. Ye, Y.X. Han, J.B. Tang, Y. Piao, X.R. Liu, Z.X. Zhou, J.Q. Gao, J.H. Rao, Y.Q. Shen, A Tumor-Specific Cascade Amplification Drug Release Nanoparticle for Overcoming Multidrug Resistance in Cancers, Adv Mater, 29 (2017).

[32] X.G. Chen, F. Liu, X.F. Song, Z.H. Wang, Z.Q. Dong, Z.Q. Hu, R.Z. Lan, W. Guan, T.G. Zhou, X.M. Xu, H. Lei, Z.Q. Ye, E.J. Peng, L.H. Du, Q.Y. Zhuang, Rapamycin regulates Akt and ERK phosphorylation through mTORC1 and mTORC2 signaling pathways, Mol Carcinog, 49 (2010) 603-610.

[33] Y.M. Ham, S.J. Mahoney, Compensation of the AKT signaling by ERK signaling in transgenic mice hearts overexpressing TRIM72, Exp Cell Res, 319 (2013) 1451-1462.

[34] S. Svenson, D.A. Tomalia, Dendrimers in biomedical applications--reflections on the field, Adv Drug Deliv Rev, 57 (2005) 2106-2129.

[35] E.A. Perez, A. Awada, J. O'Shaughnessy, H.S. Rugo, C. Twelves, S.A. Im, P. Gomez-Pardo, L.S. Schwartzberg, V. Dieras, D.A. Yardley, D.A. Potter, A. Mailliez, A. Moreno-Aspitia, J.S. Ahn, C. Zhao, U. Hoch, M. Tagliaferri, A.L. Hannah, J. Cortes, Etirinotecan pegol (NKTR-102) versus treatment of physician's choice in women with advanced breast cancer previously treated with an anthracycline, a taxane, and capecitabine (BEACON): a randomised, open-label, multicentre, phase 3 trial, Lancet Oncol, 16 (2015) 1556-1568.

[36] A.V. Kamath, J. Wang, F.Y. Lee, P.H. Marathe, Preclinical pharmacokinetics and in vitro metabolism of dasatinib (BMS-354825): a potent oral multi-targeted kinase inhibitor against SRC and BCR-ABL, Cancer Chemoth Pharm, 61 (2008) 365-376.

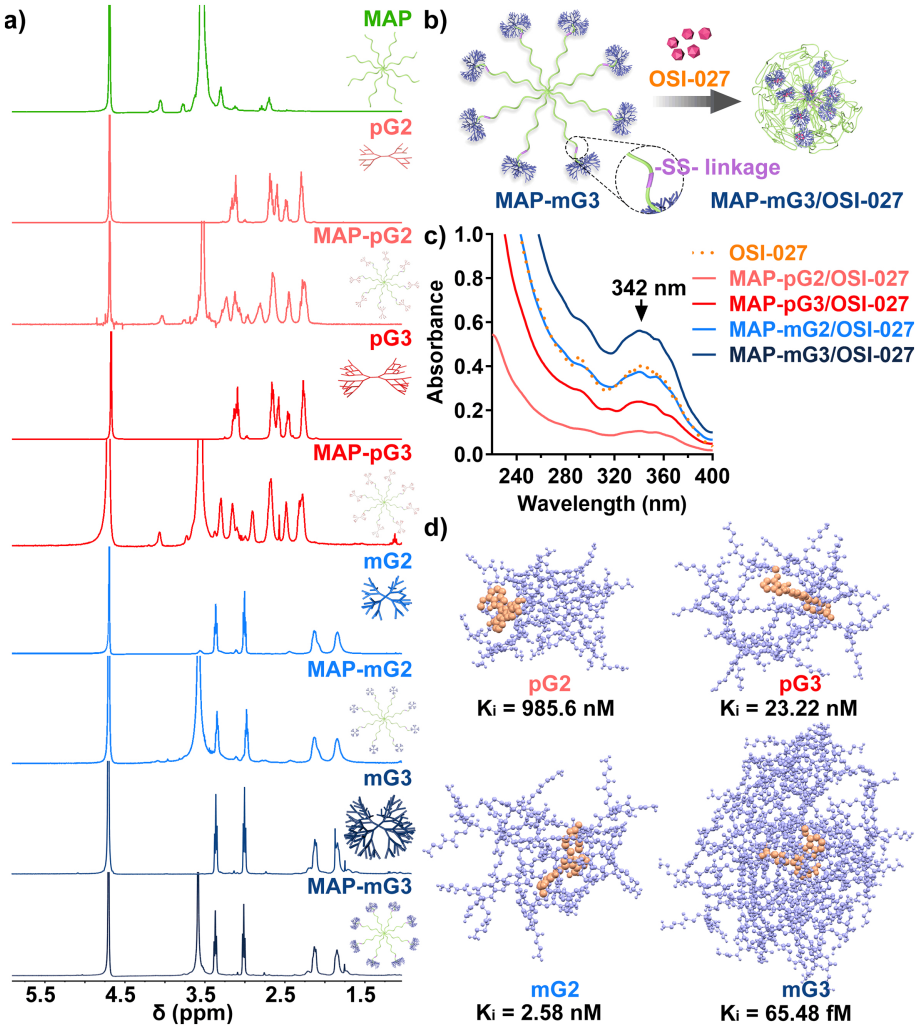
a)
MAP
pG2
MAP-pG2
pG3
MAP-pG3
mG2
MAP-mG2
mG3
MAP-mG3
5.5
4.5
3.5
2.5
1.5
δ (ppm)
b)
OSI-027
-SS- linkage
MAP-mG3
MAP-mG3/OSI-027
c)
Absorbance
1.0
0.8
0.6
0.4
0.2
0.0
240
280
320
360
400
Wavelength (nm)
342 nm
OSI-027
MAP-pG2/OSI-027
MAP-pG3/OSI-027
MAP-mG2/OSI-027
MAP-mG3/OSI-027
d)
pG2
Ki = 985.6 nM
pG3
Ki = 23.22 nM
mG2
Ki = 2.58 nM
mG3
Ki = 65.48 fM

Figure 1

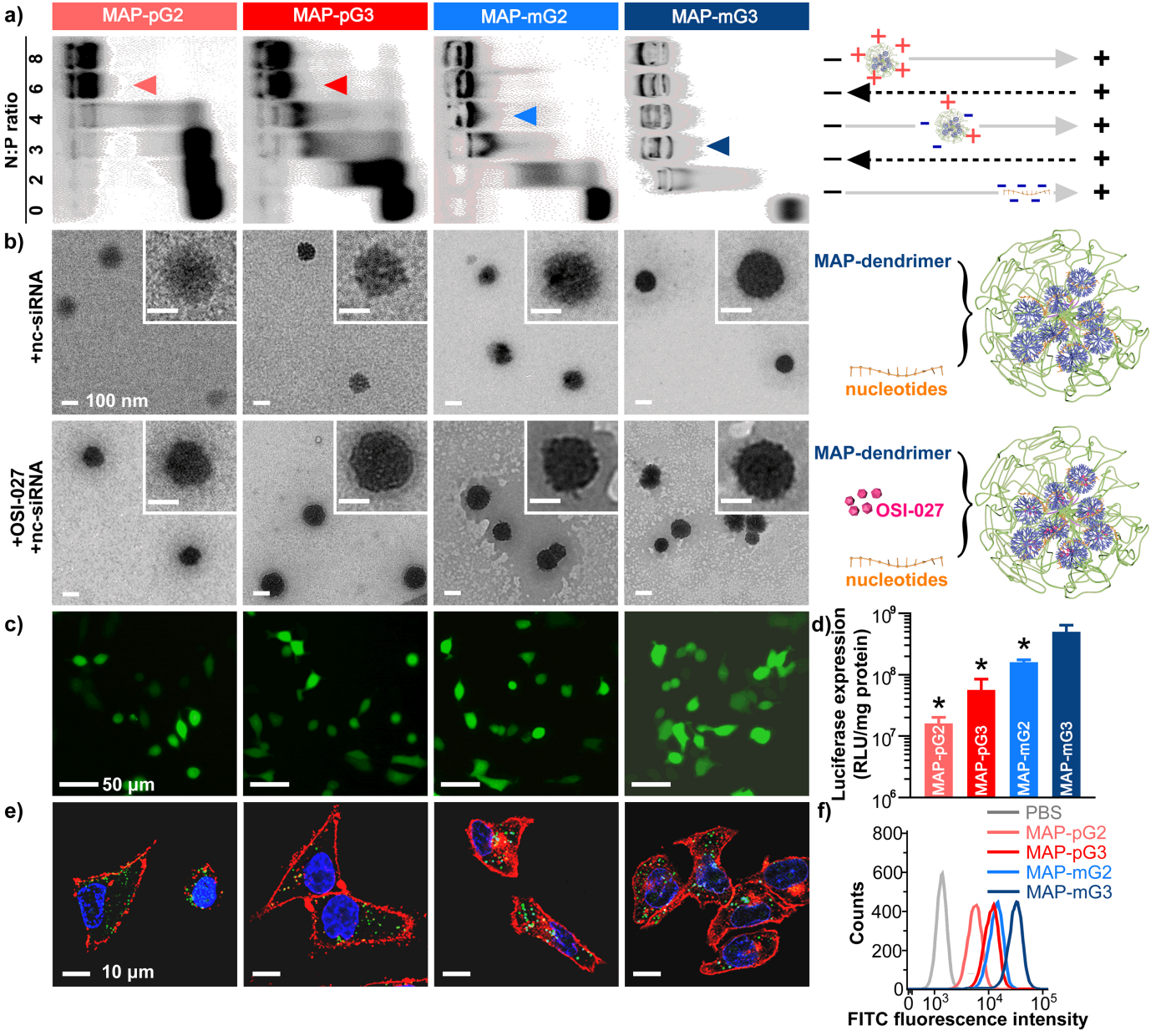
a)
MAP-pG2
MAP-pG3
MAP-mG2
MAP-mG3
N:P ratio
0
2
3
4
6
8
b)
+nc-siRNA
100 nm
+OSI-027
+nc-siRNA
MAP-dendrimer
nucleotides
MAP-dendrimer
OSI-027
nucleotides
c)
50 μm
d)
Luciferase expression
(RLU/mg protein)
10^9
10^8
10^7
10^6
*
*
*
MAP-pG2
MAP-pG3
MAP-mG2
MAP-mG3
e)
10 μm
f)
PBS
MAP-pG2
MAP-pG3
MAP-mG2
MAP-mG3
Counts
800
600
400
200
0
0
10^3
10^4
10^5
FITC fluorescence intensity

Figure 2

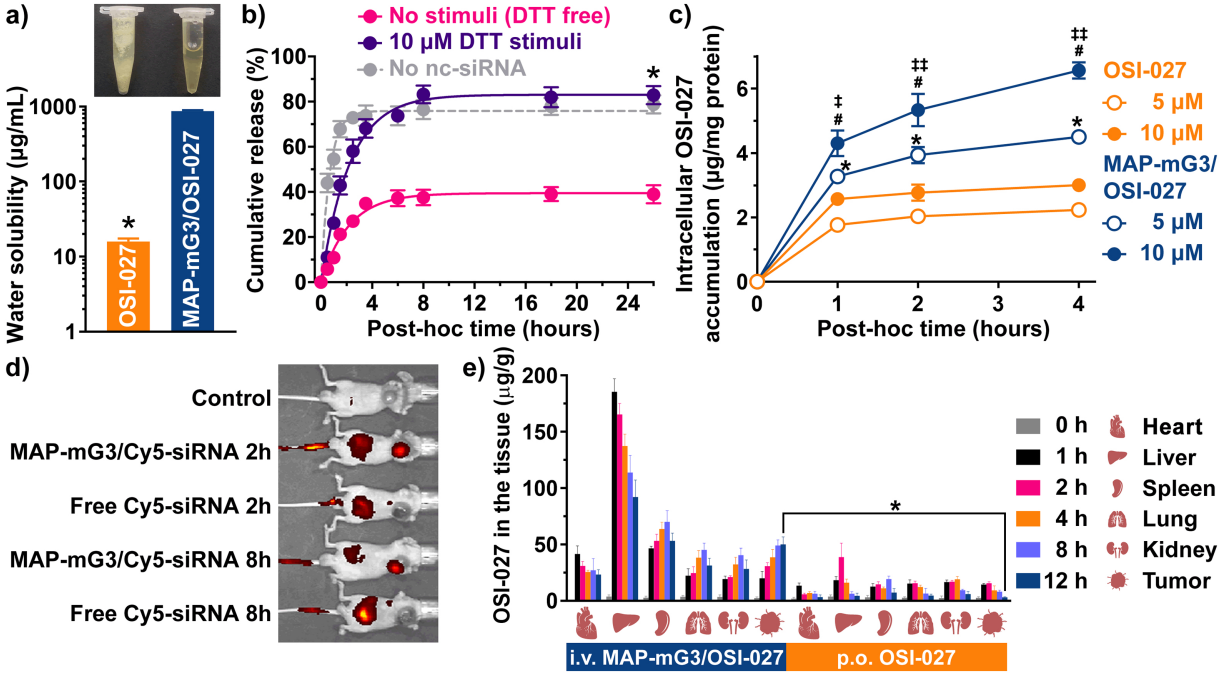
a)
Water solubility (μg/mL)
1000
100
10
1
*
OSI-027
MAP-mG3/OSI-027
b)
No stimuli (DTT free)
10 μM DTT stimuli
No nc-siRNA
Cumulative release (%)
100
80
60
40
20
0
*
0
4
8
12
16
20
24
Post-hoc time (hours)
c)
Intracellular OSI-027 accumulation (μg/mg protein)
6
4
2
0
‡
#
‡‡
#
‡‡
#
*
*
*
0
1
2
3
4
Post-hoc time (hours)
OSI-027
5 μM
10 μM
MAP-mG3/ OSI-027
5 μM
10 μM
d)
Control
MAP-mG3/Cy5-siRNA 2h
Free Cy5-siRNA 2h
MAP-mG3/Cy5-siRNA 8h
Free Cy5-siRNA 8h
e)
OSI-027 in the tissue (μg/g)
200
150
100
50
0
*
0 h
1 h
2 h
4 h
8 h
12 h
Heart
Liver
Spleen
Lung
Kidney
Tumor
i.v. MAP-mG3/OSI-027
p.o. OSI-027

Figure 3

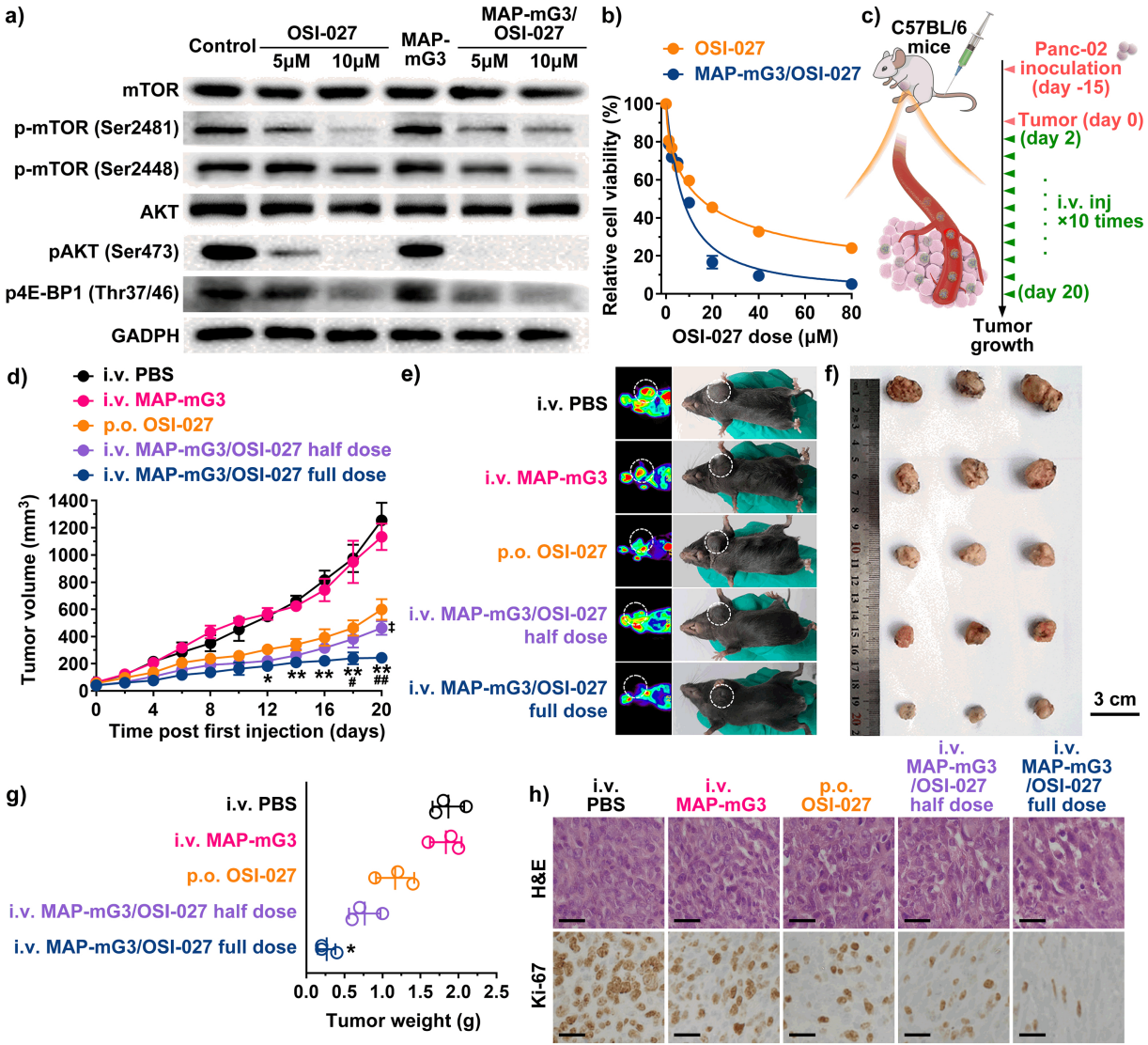
a)
Control
OSI-027
5μM
10μM
MAP-mG3
MAP-mG3/OSI-027
5μM
10μM
mTOR
p-mTOR (Ser2481)
p-mTOR (Ser2448)
AKT
pAKT (Ser473)
p4E-BP1 (Thr37/46)
GADPH
b)
OSI-027
MAP-mG3/OSI-027
Relative cell viability (%)
OSI-027 dose (μM)
c)
C57BL/6 mice
Panc-02 inoculation (day -15)
Tumor (day 0)
(day 2)
i.v. inj ×10 times
(day 20)
Tumor growth
d)
i.v. PBS
i.v. MAP-mG3
p.o. OSI-027
i.v. MAP-mG3/OSI-027 half dose
i.v. MAP-mG3/OSI-027 full dose
Tumor volume (mm3)
Time post first injection (days)
e)
i.v. PBS
i.v. MAP-mG3
p.o. OSI-027
i.v. MAP-mG3/OSI-027 half dose
i.v. MAP-mG3/OSI-027 full dose
f)
3 cm
g)
i.v. PBS
i.v. MAP-mG3
p.o. OSI-027
i.v. MAP-mG3/OSI-027 half dose
i.v. MAP-mG3/OSI-027 full dose
Tumor weight (g)
h)
i.v. PBS
i.v. MAP-mG3
p.o. OSI-027
i.v. MAP-mG3 /OSI-027 half dose
i.v. MAP-mG3 /OSI-027 full dose
H&E
Ki-67

Figure 4

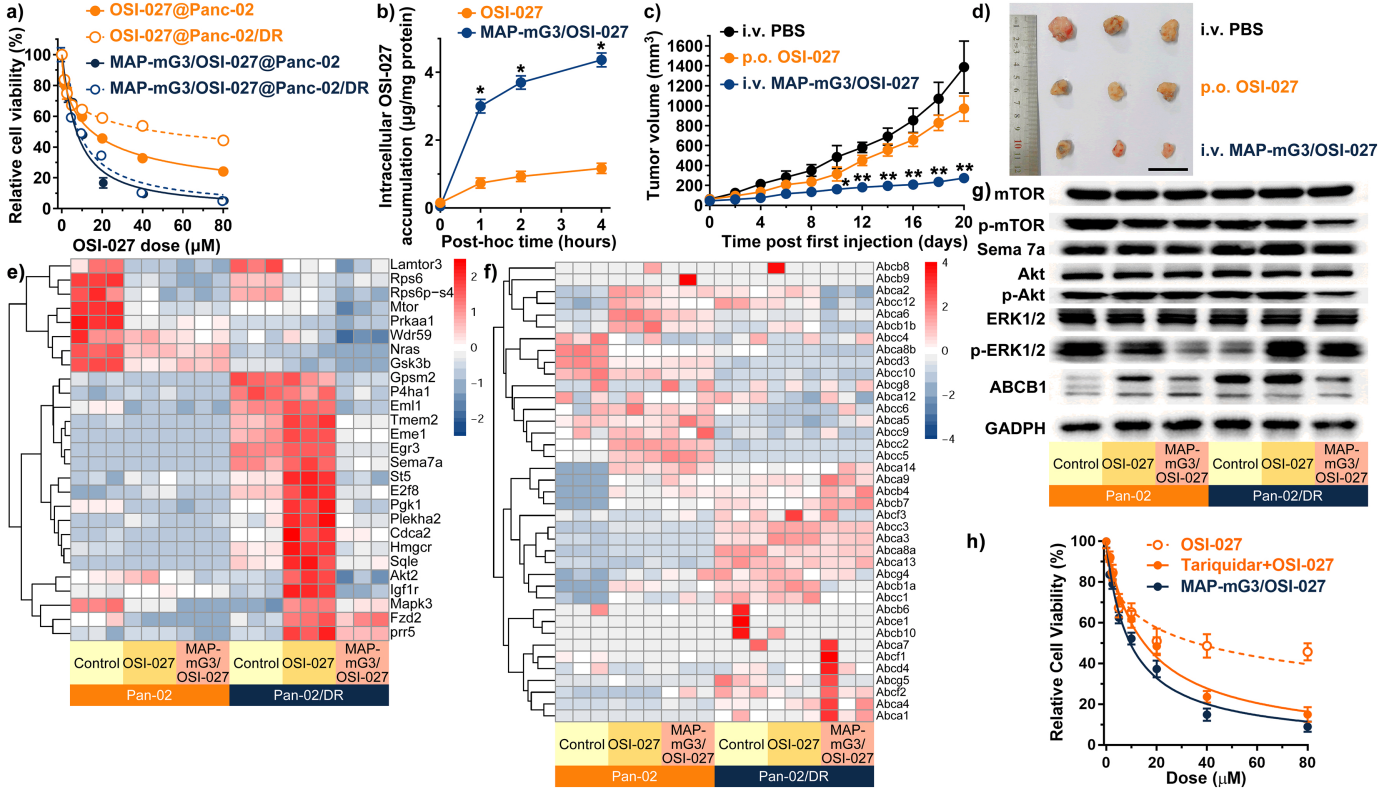
a)
OSI-027@Panc-02
OSI-027@Panc-02/DR
MAP-mG3/OSI-027@Panc-02
MAP-mG3/OSI-027@Panc-02/DR
Relative cell viability (%)
OSI-027 dose (μM)
b)
OSI-027
MAP-mG3/OSI-027
Intracellular OSI-027 accumulation (μg/mg protein)
Post-hoc time (hours)
c)
i.v. PBS
p.o. OSI-027
i.v. MAP-mG3/OSI-027
Tumor volume (mm3)
Time post first injection (days)
d)
i.v. PBS
p.o. OSI-027
i.v. MAP-mG3/OSI-027
e)
Lamtor3
Rps6
Rps6p−s4
Mtor
Prkaa1
Wdr59
Nras
Gsk3b
Gpsm2
P4ha1
Eml1
Tmem2
Eme1
Egr3
Sema7a
St5
E2f8
Pgk1
Plekha2
Cdca2
Hmgcr
Sqle
Akt2
Igf1r
Mapk3
Fzd2
prr5
Control
OSI-027
MAP-mG3/OSI-027
Pan-02
Pan-02/DR
f)
Abcb8
Abcb9
Abca2
Abcc12
Abca6
Abcb1b
Abcc4
Abca8b
Abcd3
Abcc10
Abcg8
Abca12
Abcc6
Abca5
Abcc9
Abcc2
Abcc5
Abca14
Abca9
Abcb4
Abcb7
Abcf3
Abcc3
Abca3
Abca8a
Abca13
Abcg4
Abcb1a
Abcc1
Abcb6
Abce1
Abcb10
Abca7
Abcf1
Abcd4
Abcg5
Abcf2
Abca4
Abca1
g)
mTOR
p-mTOR
Sema 7a
Akt
p-Akt
ERK1/2
p-ERK1/2
ABCB1
GADPH
h)
OSI-027
Tariquidar+OSI-027
MAP-mG3/OSI-027
Relative Cell Viability (%)
Dose (μM)

Figure 5